

Responses to Referee #1

This paper provides a detailed study of trace gases and meteorology at two sites, one a suburban site in Hong Kong (labelled TC), the other a coastal site (labelled WS), with few local anthropogenic emissions, on the edge of the South China Sea. The sites are separated by ~ 40 km. Emphasis is given to ozone episodes (>100 ppbv) and near episodes, which occurred on a number of occasions, some extending over 9 days, during two ~50 day periods in August, September; October, November 2013. The results are rationalised in detail using a range of modelling techniques: a zero dimensional box model study using the master chemical mechanism (MCM); the Weather Research and Forecasting (WRF) model to provide wind fields and coupled with the CMAQ model to provide an Eulerian representation of the physical and chemical processes over a wide area and HYSPLIT to provide backward particle release simulations to understand air mass origins. The paper provides a very useful dataset and an interesting analysis.

Thanks for the positive comments and the concerns, which helped to improve the manuscript substantially. Responses are given item by item below following the specific comments, and revisions are made where necessary.

1. The results are discussed in terms of the interaction between marine and continental air. The episodic ozone concentrations are significantly higher at WS than at TC and much of the paper relates to a discussion of the origin of these differences, which are ascribed to weaker NO titration and to a stronger oxidative capacity at the coastal site. The main meteorological features during the episodes were tropical cyclones, with transport from the polluted Pearl River Delta Region to the sites, continental anticyclones, which again brought air from polluted inland areas and Sea Land Breezes, with alternation of onshore and offshore winds.

My main concern is with the contention that the results relate to the interaction between marine and continental air, which is included in the title and pervades the text. WS is one of several islands lying close to the coast. Its important characteristic is that there are few local emissions so that NO_x is low. Other pollutants, CO, SO₂, NMHC show clear indications of advection of polluted air, but the concentrations are on average

lower than those found at TC. The wind patterns confirm that the air is primarily, perhaps exclusively during the episodes, of continental origin. Even the SLB winds from the sea simply advect high ozone concentrations, formed in polluted air, back to the coastal region. Marine air has much less impact than is found and has been widely discussed at, say, Mace Head in Ireland or Cape Grim in Tasmania.

The excellent comment is highly appreciated. As presented in the manuscript and summarized by the referee, this paper focused on the interaction between the continental and marine air in the coastal area of Hong Kong. The impacts of the continental air on air quality in marine boundary layer were discussed profoundly. Specifically, the polluted continental air masses were transported to the marine atmosphere under tropical cyclone, continental anticyclone and land breeze (section 3.2). As a result, the chemical compositions of the marine air changed substantially, leading to increased O₃ production under northerly winds at the reception of continental air (section 3.3). This process was further confirmed by the chemical transport model (section 3.4).

However, as concerned by the referee, we agree that the impacts of marine air on continental air quality were not discussed in such a comprehensive way. In fact, this effect was mainly described as sea breeze (section 3.2.3) and the intrusion of high O₃ formed over South China Sea into the continental area under sea breeze (section 3.4). In the revised manuscript, the alleviation of continental air pollution under oceanic flow is discussed, which represents a type of interaction between the continental and marine air. Furthermore, the enhancements of oceanic emission tracers (*e.g.* dimethyl sulfide) in the inland area under sea breeze are presented as an indication of marine influence. This is consistent with the findings at Mace Head in Ireland and Cape Grim in Tasmania. At last, what we want to emphasize is that this study focuses on O₃ pollution under the interaction between continental and marine air. The advection of marine air laden with O₃ back to the coastal areas is a typical interaction in this region, which is thought to be an important marine influence.

Revisions are made in the revised manuscript as follows.

The arrival of oceanic air masses generally brings substantial marine-originated compounds (e.g. dimethyl sulfide) to the continent and significantly alleviates the anthropogenic air pollution there. In fact, this is one of the main reasons for low O₃ mixing ratio observed in the PRD region in summertime when southwestern winds prevail (Wang et al., 2009; Wang et al., 2017a). In this study, it was also found that winds over the ocean increased the concentration of dimethyl sulfide at TC (see Figure S8) and reduced the levels of almost all man-made air pollutants in many cases, mainly in summertime (Figure 2a). In contrast, sea breezes carrying elevated O₃ formed over SCS might build up the terrestrial O₃ in the coastal area in some cases.

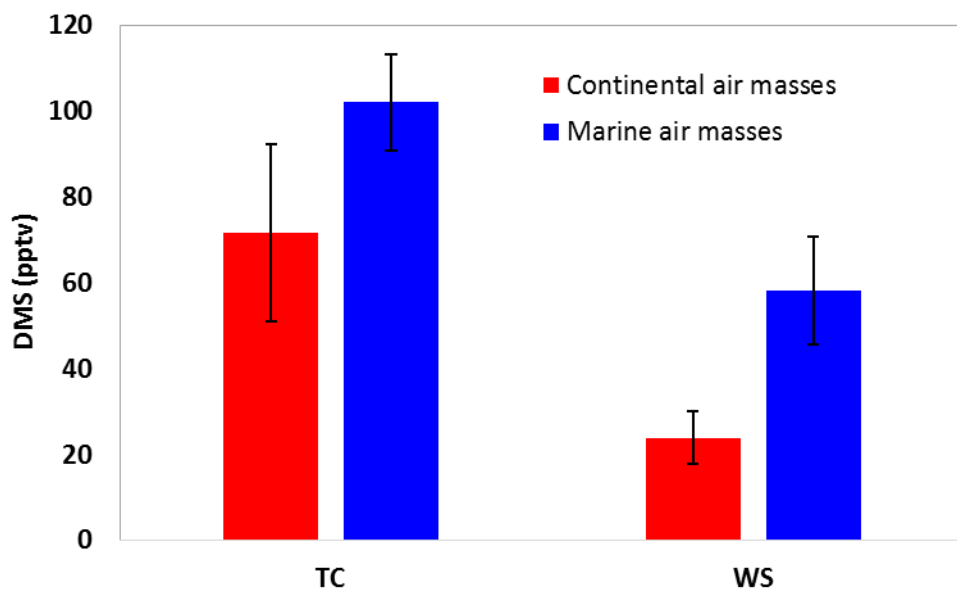


Figure S8 Average concentrations of dimethyl sulfide (DMS) observed at TC and WS when continental or marine air masses dominate.

For details, please refer to Page 29, Lines 2-11 in the revised manuscript and in the supplement.

2. The observation of higher ozone at WS compared with TC derives primarily, as argued, from the low emissions at WS and the consequently much lower NO_x and reduced titration via NO + O₃. The most telling observation is the near equivalence of

the total oxidant concentration at the two sites during both episodes and non-episodes (p 20). Similar behaviour is of course found in many other locations when comparing rural and urban ozone concentrations in similar air masses. It is the absence of local NO_x emissions at WS that leads to the differences; it is not specifically related to its coastal location and certainly not to marine influences.

Thanks for the comments. We agree that, due to the influence of NO titration, the near equivalence of the total oxidant concentration is common between two sites where primary air pollutants are intensively emitted at one site and then transported to the other site. Indeed, the similar behavior at WS and TC was partially attributable to this effect (see section 3.3.2). However, this study also demonstrated that the more intensive in-situ O_3 formation due to the stronger oxidative capacity of the atmosphere could be another important factor for the higher O_3 at WS (see section 3.3.3). Additionally, O_3 formed during the transport of polluted air masses from the continent to the marine atmosphere might also elevate O_3 at WS, which will be discussed in a companion paper (Wang et al., 2018). In fact, wherever the observed O_3 was formed, *i.e.* at WS or during the transport of air masses from the inland area to WS, the high O_3 at WS was a reflection of the interaction between the continental and marine air, because WS was nearly free of anthropogenic emissions where O_3 and its precursors were originated from the continent. Certainly, this interaction was mainly manifested as the impacts of continental air on marine air quality. We understood that the marine influences should be emphasized as a part of interaction between the continental and marine air. As responded to the previous comment (comment #1), discussions on the marine influences are extended in the revised manuscript.

3. The discussion of the daily ozone profile could also be improved. The diurnal variation is superimposed on a residual night-time ozone concentration, which is substantial, Figs 2 and S4. This might be discussed.

Many thanks for the comment. The suggested discussion has been provided in the revised manuscript.

In this study, the average NO mixing ratio at TC was 14.0 ± 0.8 ppbv, compared to 0.7 ± 0.1 ppbv at WS (Table 1). The much lower NO at WS implied weaker titration to O₃, which enabled the survival of more O₃ and caused substantial residual O₃ at WS particularly at night time when there were no photochemical reactions (Figure 2 and Figure S6).

For details, please refer to Page 21, Lines 9-12.

4. Is the higher rate of ozone formation, shown in Fig 5b, a reflection of the high ozone concentration itself? It would be helpful to show the concentrations of OH, HO₂ and RO₂ vs time and also their rates of production and loss. Is the enhanced [OH] a result of increased O¹D production from the higher [O₃] found at WS in episodes? These plots could, if necessary, be shown in the Supplement.

We are grateful for the good comments. The higher net O₃ production during O₃ episodes at WS, as shown in Figure 5 (b) of the original manuscript, was directly caused by the enhanced reaction rates of RO₂+NO and HO₂+NO. This was associated with the increase of O₃ precursors, particularly NO_x, during O₃ episodes. Under the assumption that local O₃ formation dominated O₃ budget at WS, the higher O₃ production rate during O₃ episodes resulted in higher O₃, or it was a reflection of the higher O₃. However, the higher O₃ production rate was not caused by the higher observed O₃ during episodes, which were not input into the model.

As suggested, the concentrations of OH, HO₂ and RO₂, as well as their production and loss rates, are presented in the revised supplement with discussions in the revised manuscript. The enhanced [OH] during O₃ episodes cannot be totally attributable to the increased O¹D (O₃ photolysis). Instead, most of the OH increase was attributable to the enhanced reaction rate between HO₂ and NO during O₃ episodes.

O₃ formation is driven by the transformation and recycling of oxidative radicals, including OH, HO₂ and RO₂, collectively referred to as RO_x hereafter. The production and loss rates of these radicals, and their equilibrium concentrations on the canister sampling days were simulated by the PBM-MCM model, as shown in Figure S7. We noticed that WS featured significantly higher levels of these oxidative radicals on average ($p < 0.05$). The daytime (7:00-19:00 LT) average OH

concentration at TC and WS was $(1.5 \pm 0.4) \times 10^6$ molecules cm^{-3} and $(5.5 \pm 0.9) \times 10^6$ molecules cm^{-3} during O_3 episodes, respectively. Consistently, HO_2 and RO_2 at WS were well above those at TC (Table 3). This pattern was also applicable between the two sites during non-episodes. Furthermore, while the difference in OH concentration became less on non-episode days, the gaps for peroxy radicals (HO_2 and RO_2) between TC and WS widened, as listed in Table 3. From non-episodes to episodes, OH increased at WS alongside with the decreases of HO_2 and RO_2 , likely indicating more conversion of HO_2 to OH by NO, which is an important pathway leading to O_3 formation. Details about this were shown later.

To explain the inter-site differences of the concentrations of oxidative radicals and the variations between O_3 episodes and non-episodes, Figure S7 also provides the breakdowns of the production and loss rates of OH, HO_2 and RO_2 at TC and WS, separately. Overall, the reaction between HO_2 and NO dominated the production of OH at both sites, with the contribution of $69.4 \pm 2.0\%$ and $81.0 \pm 1.5\%$ at TC and WS, respectively. While the photolysis of HONO ranked the second in the production of OH at TC ($22.2 \pm 2.1\%$), the contribution of this pathway to OH production at WS ($3.7 \pm 0.6\%$) was overstepped by O_3 photolysis ($13.1 \pm 1.6\%$). This discrepancy was associated with the higher HONO and lower O_3 at TC (Figure S1 and Table 3). As expected, the production rate of OH through HO_2 reacting with NO experienced the most significant increase from $1.4 \pm 0.2 \times 10^7$ molecules $\text{cm}^{-3} \text{ s}^{-1}$ during non-episodes to $3.6 \pm 0.6 \times 10^7$ molecules $\text{cm}^{-3} \text{ s}^{-1}$ during O_3 episodes at WS, which explained more than 90% of the increase of the total OH production. In terms of the losses of OH, reaction between OH and NO_2 was the largest sink of OH at TC. However, OH-initiated oxidations of VOCs consumed most ($52.7 \pm 1.8\%$) of OH at WS. This was reasonable in view of the much more abundant NO_2 at TC than at WS, in contrast to the smaller difference in NMHCs between the two sites (Table 3). Since OH can generally be recycled from the oxidation of VOCs, the lower OH at TC was likely caused by the lower O_3 photolysis and higher consumption of OH by NO_2 , despite the more intensive HONO photolysis. The overall oxidation rate of VOCs by OH was employed to indicate the atmospheric oxidative capacity in previous studies (Elshorbany et al., 2009; Xue et al., 2016). In this study, we found that the oxidation rate of VOCs at TC ($6.1 \pm 2.1 \times 10^6$ molecules $\text{cm}^{-3} \text{ s}^{-1}$ during O_3 episodes and $5.7 \pm 0.9 \times 10^6$ molecules $\text{cm}^{-3} \text{ s}^{-1}$ during non-episodes) was remarkably ($p < 0.05$) lower than that at WS (O_3 episode: $15 \pm 2.5 \times 10^6$ molecules $\text{cm}^{-3} \text{ s}^{-1}$ and non-episode: $8.9 \pm 1.3 \times 10^6$ molecules $\text{cm}^{-3} \text{ s}^{-1}$). The results revealed that the atmospheric oxidative capacity at TC was weaker than at WS for

both O₃ episodes and non-episodes, inconsistent with the findings of Elshorbany et al. (2009) and Xue et al. (2016) who concluded that the atmospheric oxidative capacity was higher in more polluted environments due to the fact that the atmospheric oxidative capacity is positively proportional to the VOCs and OH levels. Both Elshorbany et al. (2009) and Xue et al. (2016) reported very high mixing ratios of VOCs (*e.g.* toluene of 9.5 and 6.3 ppbv, respectively) in the polluted cases, which explained the strong atmospheric oxidative capacity. However, in this study, it is more likely that the higher NO_x at TC consumed more OH and resulted in lower oxidative capacity than at WS, despite the slightly higher VOCs at TC (Table 3).

For HO₂, RO₂ reacting with NO accounted for 56.7±1.1% and 60.7±1.0% of HO₂ production at TC and WS, respectively. Oxidation of CO by OH was also an important pathway leading to HO₂ formation, second to RO₂+NO at both sites. At TC, HO₂ was almost exclusively depleted by NO. However, 10.8±1.8% and 6.5±0.8% of the HO₂ losses were attributable to HO₂-RO₂ and HO₂-HO₂ reactions at WS, respectively, though HO₂+NO was responsible for the most fraction (82.7±2.6%) of HO₂ losses. We believe that the more significant self-consumption of peroxy radicals at WS was closely related to the low NO_x there, which hampered the transfer of oxygen atom from peroxy radicals to NO and further formation of O₃. This was confirmed by the enhanced losses of HO₂ through reactions with HO₂ itself and RO₂ from 3.0±1.2% during O₃ episodes to 24.9±3.4% during non-episodes at WS, because NO_x was more scarce during non-episodes at this site (Table 3). Similarly, in contrast to the negligible influence of RO₂ reacting with HO₂ on RO₂ budget at TC, HO₂-RO₂ reactions played important role in losses of RO₂ at WS, particularly on non-episode days (Figure S7). When OH, HO₂ and RO₂ were summed up, the production and loss rate of RO_x were obtained, as shown in Figure 5(a). Under such circumstance, the transformation and recycling pathways among these radicals can be neglected. For example, OH-initiated oxidation of VOCs consumes OH, which however generates RO₂. Therefore, these reactions were not considered as sources or sinks of RO_x. On one hand, HONO photolysis was the largest source of RO_x at TC (53.7±2.6%), followed by the photolysis of HCHO (21.1±1.6%) and O₃ (18.7±1.5%). However, O₃ photolysis ranked the first among the sources of RO_x at WS with the contribution of 38.6±2.3%, higher than the contributions from HCHO photolysis (34.3±1.4%) and HONO photolysis (18±2.5%). On the other hand, while the reaction between OH and NO₂ served as the sole sink of RO_x at TC, it only explained 50% of RO_x sink at WS with the other half attributable to self-consumption of peroxy radicals.

For details, please refer to Section 3.3.3 (Page 22) and Figure 5 in the revised manuscript and Figure S7 in the revised supplement.

5. It would also be helpful, again in the Supplement, to see ozone, OH, HO₂ and RO₂ concentrations, and ozone and radical rates of formation and loss on a specific episode day. Using averages can lead to a loss of clarity and understanding.

Thanks for the suggestion. The concentrations and formation/loss rates of radicals, *i.e.* OH, HO₂ and RO₂, and O₃ are provided on daily basis in the revised manuscript and revised supplement. More discussions are given for better understanding of the photochemistry.

For details, please refer to the responses to comment #4.

6. Two additional points: O₁D in the caption to Fig 5 should be O¹D. The English needs a good deal of attention, particularly the frequent absence of definite / indefinite articles. Sorry for the mistake in O₁D, which is corrected to O¹D throughout the manuscript. The English, particularly the absence of definite/indefinite articles, has been double checked and revised where necessary.

7. The paper makes a substantial contribution and should be published in ACP. The authors, though, should consider the points made above relating to the overall emphasis of the paper and the clarity of the discussion on chemical processes.

Thanks again for the positive comments on the paper. Revisions are made according to the comments and suggestions, which mainly include the discussions on marine influences and chemical processes at both sites. We hope that the revised manuscript is satisfactory to the referee.

Responses to Referee #2

This paper reports intensive field measurements at two sites over the South China Sea. The spatial distribution of ozone pollution and its favorable synoptic conditions were interpreted. The authors also tried to link, by the sea-land breeze, the transport of continental pollution to oceans and the recirculation of land-originated aged air masses from ocean to the coastal regions. The manuscript is generally well written and easy to follow. The following specific comments should be addressed before it can be considered for publication at ACP.

Specific Comments:

1. Page 1, Line 6: Hong Kong, China.

Thanks for the comment. The author's address has been amended.

2. Page 2, Lines 5-6: the authors may either spell out TC and WS, or just remove them from the abstract.

Thanks for the suggestion. The sampling sites (i.e. TC and WS) have been spelled out.

3. Page 2, Line 15: the word "magnified" may be not appropriate here. The ozone-laden air may be transported to a larger area over the oceans, but should not be "magnified".

Thanks for the Referee's concern. Since this study successfully demonstrates O₃ concentration and production increased at the marine site due to the strong atmospheric oxidative capacity as well as the changed chemical compositions at the reception of continental air, the authors think that the use of "magnified" here is not improper.

4. Page 3, Lines 14-19: to date, the long-term O₃ trend studies were relatively limited in

China. The authors should refer to the following earlier studies in Hong Kong, the PRD region and northern China.

Sun, et al., Significant increase of summertime ozone at Mount Tai in Central Eastern China, *Atmos. Chem. Phys.*, 16, 10637-10650, 2016.

Xue et al., Increasing external effects negate local efforts to control ozone air pollution: a case study of Hong Kong and implications for other Chinese cities, *Environ. Sci. Tech.*, 48, 10769-10775, 2014.

Thanks for providing these references. They have been cited in the revised manuscript.

“However, increasing studies showed that surface O₃ was elevated rapidly in East Asia in the last decade (Ding et al., 2008; Xu et al., 2008; Parrish et al., 2012; **Xue et al., 2014**; Zhang et al., 2014; **Sun et al., 2016**; Lin et al., 2017; Wang et al., 2017a). For example, the observational data revealed that regional O₃ concentrations increased at a rate of 0.86 ppbv yr⁻¹ in Pearl River Delta (PRD) from 2006 to 2011 (Li et al., 2014), at a rate of 0.56 ppbv yr⁻¹ in Hong Kong from 2005 to 2014 (Wang et al., 2017a), **and even at a rate of 1.7-2.1 ppbv yr⁻¹ (summertime only) at Mount Tai in central eastern China (Sun et al., 2016).**”

For details, please refer to page 3, lines 13-20.

5. Page 4, Lines 24-26: a more recent study has investigated the detailed chemical features including the radical chemistry in different air masses arriving at the South China Sea.

Li et al., Oxidizing capacity of the rural atmosphere in Hong Kong, Southern China. *Science of the Total Environment*. 612. 1114-1122. 2018.

Thanks for providing this new reference. Li et al. (2018) has been cited in the revised manuscript.

So far, only a handful of studies deeply evaluated the chemical characteristics of air masses under various synoptic systems (Wang et al., 2005; Guo et al., 2009; Guo et al., 2013; Li et al., 2018).

For details, please refer to Page 4, Lines 26-28.

6. Page 5, Lines 21-22: it is not the case that northeast monsoon prevails in late summer. The O₃ episode occurring in late summer in Hong Kong is mainly related to the tropical cyclones.

Yes, tropical cyclones are one of the principal factors leading to O₃ episodes occurring in late summer and autumn in Hong Kong, which has been acknowledged in the Section 3.2 in the original manuscript. In addition, northeast monsoon prevailing in autumn would also contribute to high O₃ mixing ratio observed in Hong Kong by bringing in high concentrations of O₃ and its precursors from the PRD and other heavy-polluted areas. To make this point clearer, the sentence has been revised and now reads as follows:

High O₃ mixing ratios are frequently observed in Hong Kong in late summer and autumn (Ling et al., 2013) when tropical cyclones and the northeast monsoon prevail, respectively.

For details, please refer to Page 5, Lines 27-28.

7. Page 6, Lines 8-10: it has been known that the traditional commercial NO_x analyzer may be subject to significant positive interference for the NO₂ measurements, especially at the rural and remote areas like WS. The authors need state the uncertainty of the NO₂ measurements and the subsequent observation-based modeling analysis.

Thanks for the comment. The uncertainty of the NO_x measurements has been added in the method section.

It was noteworthy that the measured NO_x might include other oxidized reactive nitrogen that was converted by the molybdenum. Thus, the NO_x concentrations given below

were considered the upper limits of their actual values (Dunlea et al., 2007; Ran et al., 2011).

In addition, the inherent uncertainty of NO_x measurement mentioned above might slightly affect the modeling results.

For details, please refer to Page 6, Lines 12-15 and Page 9, Lines 9-10.

8. Page 8, Lines 16-18: so the OBM was not constrained by the measured HONO and OVOCs, right? This may affect the accurate modeling of OH radicals and ozone formation. As the OVOC measurements were available in the present study, the authors should constrain the model with the measured OVOC data.

Thanks for the comment. The measured OVOCs, as well as the HONO obtained from previously published data, have been used to constrain the OBM. The new results are presented in the revised manuscript. Please see Comment 13 for more details.

9. Page 9, Lines 19-27: it would be better if the authors could provide the time series of model simulations and observations for a direct comparison, maybe in the supporting information.

Thanks for the good suggestion. For comparison, the time series of model simulations and observations have been added in Figure S3 in the revised supplement.

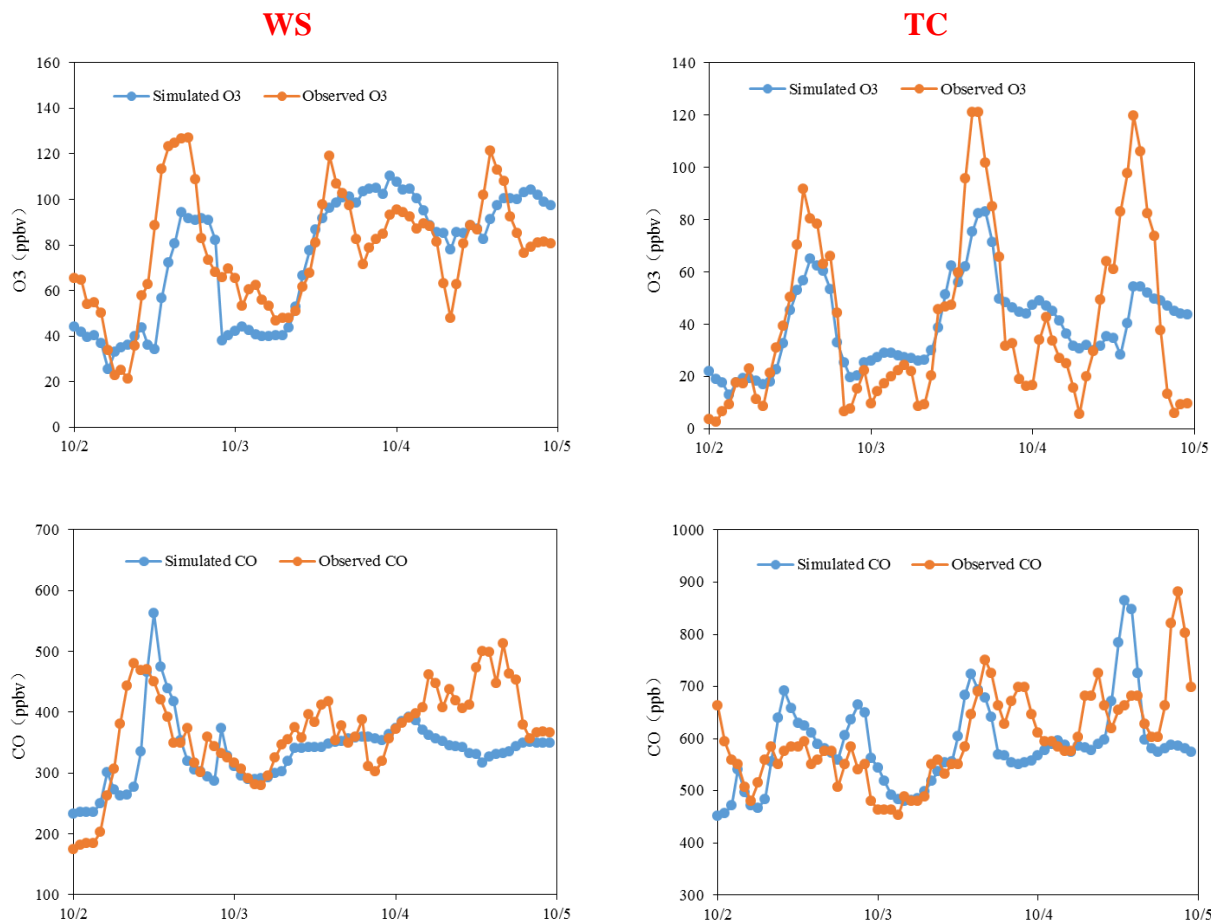


Figure S3. Time series of the WRF-CMAQ simulated and the observed CO and O₃ at WS (left panel) and TC (right panel) during a typical O₃ episode on Oct. 2-4, 2013.

10. Page 10, Table 1: it would be much better if the statistics of the most abundant NHMC and carbonyl species are individually shown, instead of the bulk concentrations.

Thanks for the suggestion. The statistics of the top 10 NHMC and the top 3 carbonyl species are individually shown in Table S5 in the revised supplement.

Table S5. Statistics (Mean \pm 95% C.I.) of the top 10 NMHC and the top 3 carbonyl species observed at TC and WS during O₃ episodes and non-episodes (unit: pptv).

Compound	TC		WS	
	Episode	Non-episode	Episode	Non-episode
Ethane	2179 \pm 222	1852 \pm 256	2077 \pm 182	1456 \pm 167

<i>Propane</i>	1966±277	1572±207	1523±126	866±126
<i>i-Butane</i>	1944±371	1433±166	1559±167	810±115
<i>Acetylene</i>	2083±165	1316±145	1805±133	1086±122
<i>Toluene</i>	1829±365	1357±254	1737±388	703±183
<i>n-Butane</i>	1437±163	1336±148	1160±145	480±113
<i>n-Hexane</i>	733±329	1351±443	980±299	447±121
<i>Ethene</i>	1140±167	1077±171	826±99	691±94
<i>i-Pentane</i>	964±145	813±123	918±99	523±96
<i>Benzene</i>	614±49	428±51	587±47	381±44
<i>Formaldehyde</i>	5068±454	3522±286	4257±355	2471±180
<i>Acetone</i>	5064±831	3367±445	3984±287	2086±162
<i>Acetaldehyde</i>	1807±162	1241±115	1618±133	920±105

11. Section 3.2: this section is too long and contains a lot of general description of the typhoon, continental anticyclone, and sea-land breeze (most of them are already well known). The authors may consider to further shorten such general descriptions and mainly highlight the new results obtained in this study.

Thanks for the comment. The Section 3.2 has been further shortened in the revised manuscript by removing some simple descriptive text, for example:

“The main feature of the anticyclones is sinking air at the center with gentle clockwise winds in the northern hemisphere. The air warms up as it sinks by compression leading to warm, cloudless and dry weather, which is conducive to intensive photochemical O₃ formation. In addition, anticyclone is a large-scale weather system which produces long-lasting settled and calm weather for many days or weeks favorable to the accumulation of primary and secondary pollutants.” and

“In general, the temperature difference between the sea and the land is large on the SLB days. Taking 3 Oct. as an example, the maximum hourly temperature at TC was

3.2 °C higher than that at WS during daytime hours, whereas the minimum hourly temperature in the evening was 2.7 °C lower at TC than at WS.”

For details, please refer to Section 3.2 (Pages 14-19) in the revised manuscript.

12. Section 3.3.3: it is not clear whether the modeling analysis was conducted for the campaign average condition or for a particular case. Furthermore, the sub-title of this section may be not appropriate as this section only talked about the simulated OH level and O₃ formation, other than the atmospheric oxidative capacity.

Thanks for the comment. The modeling analysis in section 3.3.3 was conducted for the individual days when VOCs were collected. For the subtitle, we have discussed the atmospheric oxidative capacity in the revised manuscript according to the definition in Elshorbany et al. (2009) and Xue et al. (2016), *i.e.* oxidation rate of VOCs by OH. However, since O₃ production rate is also an important content in this section, the subtitle has been changed to “Atmospheric oxidative capacity and O₃ production rate”.

3.3.3 Atmospheric oxidative capacity and O₃ production rate

O₃ formation is driven by the transformation and recycling of oxidative radicals, including OH, HO₂ and RO₂, collectively referred to as RO_x hereafter. The production and loss rates of these radicals, and their equilibrium concentrations on the canister sampling days were simulated by the PBM-MCM model, as shown in Figure S7.

For details, please refer to Page 22, Lines 20-24.

The overall oxidation rate of VOCs by OH was employed to indicate the atmospheric oxidative capacity in previous studies (Elshorbany et al., 2009; Xue et al., 2016). In this study, we found that the oxidation rate of VOCs at TC ($6.1 \pm 2.1 \times 10^6$ molecules cm⁻³ s⁻¹ during O₃ episodes and $5.7 \pm 0.9 \times 10^6$ molecules cm⁻³ s⁻¹ during non-episodes) was remarkably ($p < 0.05$) lower than that at WS (O₃ episode: $15 \pm 2.5 \times 10^6$ molecules cm⁻³ s⁻¹ and non-episode: $8.9 \pm 1.3 \times 10^6$ molecules cm⁻³ s⁻¹). The results revealed that the atmospheric oxidative capacity at TC was weaker than at WS for both O₃ episodes and non-episodes, inconsistent with the findings of Elshorbany et al. (2009) and Xue et al. (2016) who concluded that the atmospheric oxidative capacity was higher in more

polluted environments due to the fact that the atmospheric oxidative capacity is positively proportional to the VOCs and OH levels. Both Elshorbany et al. (2009) and Xue et al. (2016) reported very high mixing ratios of VOCs (*e.g.* toluene of 9.5 and 6.3 ppbv, respectively) in the polluted cases, which explained the strong atmospheric oxidative capacity. However, in this study, it is more likely that the higher NO_x at TC consumed more OH and resulted in lower oxidative capacity than at WS, despite the slightly higher VOCs at TC (Table 3).

For details, please refer to Page 23, Lines 20-33, and Page 24, lines 1-2.

13. Page 21, Lines 8-10: based on the current analysis, I don't agree that the atmospheric oxidative capacity is stronger at the coastal WS than polluted TC site. HONO photolysis is a very important OH source in polluted areas including the TC site (Xue et al., 2016), which was not included in the present study. So the OH levels should be underestimated at TC. Moreover, the lower OH levels at TC should be due to the fast radical cycling given the more abundant VOCs. I presume that the HO₂ and RO₂ levels at TC should be significantly higher than those at WS.

Xue et al., Oxidative capacity and radical chemistry in the polluted atmosphere of Hong Kong and Pearl River Delta region: analysis of a severe photochemical smog episode. *Atmospheric Chemistry and Physics*. 16. 9891-9903. 2016.

The excellent comment is highly appreciated. Firstly, HONO was indeed not input into the model for simulation of photochemistry in this study, as we did not measure HONO concentrations in the sampling campaign. We agree that the absence of HONO might have an influence on the conclusions about photochemistry at the two sites. Therefore, the average diurnal profiles of HONO observed at TC and a coastal background site (Hok Tsui, HT) in Hong Kong were used to present the average levels of HONO at TC and WS, respectively, for model simulations again.

HONO has been recognized as an important source of OH, influencing O₃ formation significantly (Kleffmann, 2007). Since we did not measure HONO mixing ratios in this study, the average diurnal profiles of HONO observed at TC in autumn 2011 (Xu et al., 2015) and at a coastal background site (Hok Tsui, HT) in southeast Hong Kong in autumn 2012 (Zha, 2015) were applied to the photochemical simulations at TC and WS, respectively. Figure S1 shows the

average diurnal cycles of HONO at TC and HT. The use of the aforementioned diurnal profiles might increase the uncertainty of model simulation. However, we believe that the newly introduced uncertainties could not be too high, because HONO observations at TC and HT were carried out 2 years and 1 year before the sampling campaign of this study, respectively. In addition, HT was comparable to WS in aspects of local emissions (nearly free of anthropogenic emissions), air mass category (mixed continental and marine air) and location (to the south of Hong Kong and on SCS).

For details, please refer to Section 2.3 (Pages 8-9).

However, with the inclusion of HONO, the simulated OH, HO₂ and RO₂ at TC were still lower than those at WS. To keep consistency with previous studies (Elshorbany et al., 2009; Xue et al. 2016), the atmospheric oxidative capacity is defined as the overall oxidation rate of VOCs by OH in the revised manuscript. We found that the atmospheric oxidative capacity was also much higher at WS than at TC, due to the higher OH concentration at WS despite the lower VOC levels. In fact, according to our analyses, the lower OH at TC was more related to the higher NO₂, which served as a scavenger of OH through the formation of HNO₃. The lower HO₂ and RO₂ at TC was possibly resulted from their conversion to OH and RO (HO₂ and OH subsequently), under the condition of sufficient NO. However, the recycled OH could be further removed by reacting with NO₂. As a consequence, OH, HO₂ and RO₂ were progressively consumed, which caused their lower concentrations at TC. This section has been substantially revised as follows.

O₃ formation is driven by the transformation and recycling of oxidative radicals, including OH, HO₂ and RO₂, collectively referred to as RO_x hereafter. The production and loss rates of these radicals, and their equilibrium concentrations on the canister sampling days were simulated by the PBM-MCM model, as shown in Figure S7. We noticed that WS featured significantly higher levels of these oxidative radicals on average ($p < 0.05$). The daytime (7:00-19:00 LT) average OH concentration at TC and WS was $(1.5 \pm 0.4) \times 10^6$ molecules cm⁻³ and $(5.5 \pm 0.9) \times 10^6$ molecules cm⁻³ during O₃ episodes, respectively. Consistently, HO₂ and RO₂ at WS were well above those at TC (Table 3). This pattern was also applicable between the two sites during non-episodes. Furthermore, while the difference in OH concentration became less on non-episode days, the

gaps for peroxy radicals (HO_2 and RO_2) between TC and WS widened, as listed in [Table 3](#). From non-episodes to episodes, OH increased at WS alongside with the decreases of HO_2 and RO_2 , likely indicating more conversion of HO_2 to OH by NO, which is an important pathway leading to O_3 formation. Details about this were shown later.

To explain the inter-site differences of the concentrations of oxidative radicals and the variations between O_3 episodes and non-episodes, [Figure S7](#) also provides the breakdowns of the production and loss rates of OH, HO_2 and RO_2 at TC and WS, separately. Overall, the reaction between HO_2 and NO dominated the production of OH at both sites, with the contribution of $69.4 \pm 2.0\%$ and $81.0 \pm 1.5\%$ at TC and WS, respectively. While the photolysis of HONO ranked the second in the production of OH at TC ($22.2 \pm 2.1\%$), the contribution of this pathway to OH production at WS ($3.7 \pm 0.6\%$) was overstepped by O_3 photolysis ($13.1 \pm 1.6\%$). This discrepancy was associated with the higher HONO and lower O_3 at TC ([Figure S1](#) and [Table 3](#)). As expected, the production rate of OH through HO_2 reacting with NO experienced the most significant increase from $1.4 \pm 0.2 \times 10^7$ molecules $\text{cm}^{-3} \text{ s}^{-1}$ during non-episodes to $3.6 \pm 0.6 \times 10^7$ molecules $\text{cm}^{-3} \text{ s}^{-1}$ during O_3 episodes at WS, which explained more than 90% of the increase of the total OH production. In terms of the losses of OH, reaction between OH and NO_2 was the largest sink of OH at TC. However, OH-initiated oxidations of VOCs consumed most ($52.7 \pm 1.8\%$) of OH at WS. This was reasonable in view of the much more abundant NO_2 at TC than at WS, in contrast to the smaller difference in NMHCs between the two sites ([Table 3](#)). Since OH can generally be recycled from the oxidation of VOCs, the lower OH at TC was likely caused by the lower O_3 photolysis and higher consumption of OH by NO_2 , despite the more intensive HONO photolysis. The overall oxidation rate of VOCs by OH was employed to indicate the atmospheric oxidative capacity in previous studies (Elshorbany et al., 2009; Xue et al., 2016). In this study, we found that the oxidation rate of VOCs at TC ($6.1 \pm 2.1 \times 10^6$ molecules $\text{cm}^{-3} \text{ s}^{-1}$ during O_3 episodes and $5.7 \pm 0.9 \times 10^6$ molecules $\text{cm}^{-3} \text{ s}^{-1}$ during non-episodes) was remarkably ($p < 0.05$) lower than that at WS (O_3 episode: $15 \pm 2.5 \times 10^6$ molecules $\text{cm}^{-3} \text{ s}^{-1}$ and non-episode: $8.9 \pm 1.3 \times 10^6$ molecules $\text{cm}^{-3} \text{ s}^{-1}$). The results revealed that the atmospheric oxidative capacity at TC was weaker than at WS for both O_3 episodes and non-episodes, inconsistent with the findings of Elshorbany et al. (2009) and Xue et al. (2016) who concluded that the atmospheric oxidative capacity was higher in more polluted environments due to the fact that the atmospheric oxidative capacity is positively proportional to the VOCs and OH levels. Both Elshorbany et al. (2009) and Xue et al. (2016)

reported very high mixing ratios of VOCs (*e.g.* toluene of 9.5 and 6.3 ppbv, respectively) in the polluted cases, which explained the strong atmospheric oxidative capacity. However, in this study, it is more likely that the higher NO_x at TC consumed more OH and resulted in lower oxidative capacity than at WS, despite the slightly higher VOCs at TC (Table 3).

For HO₂, RO₂ reacting with NO accounted for 56.7±1.1% and 60.7±1.0% of HO₂ production at TC and WS, respectively. Oxidation of CO by OH was also an important pathway leading to HO₂ formation, second to RO₂+NO at both sites. At TC, HO₂ was almost exclusively depleted by NO. However, 10.8±1.8% and 6.5±0.8% of the HO₂ losses were attributable to HO₂-RO₂ and HO₂-HO₂ reactions at WS, respectively, though HO₂+NO was responsible for the most fraction (82.7±2.6%) of HO₂ losses. We believe that the more significant self-consumption of peroxy radicals at WS was closely related to the low NO_x there, which hampered the transfer of oxygen atom from peroxy radicals to NO and further formation of O₃. This was confirmed by the enhanced losses of HO₂ through reactions with HO₂ itself and RO₂ from 3.0±1.2% during O₃ episodes to 24.9±3.4% during non-episodes at WS, because NO_x was more scarce during non-episodes at this site (Table 3). Similarly, in contrast to the negligible influence of RO₂ reacting with HO₂ on RO₂ budget at TC, HO₂-RO₂ reactions played important role in losses of RO₂ at WS, particularly on non-episode days (Figure S7). When OH, HO₂ and RO₂ were summed up, the production and loss rate of RO_x were obtained, as shown in Figure 5(a). Under such circumstance, the transformation and recycling pathways among these radicals can be neglected. For example, OH initiated oxidation of VOCs consumes OH, which however generates RO₂. Therefore, these reactions were not considered as sources or sinks of RO_x. On one hand, HONO photolysis was the largest source of RO_x at TC (53.7±2.6%), followed by the photolysis of HCHO (21.1±1.6%) and O₃ (18.7±1.5%). However, O₃ photolysis ranked the first among the sources of RO_x at WS with the contribution of 38.6±2.3%, higher than the contributions from HCHO photolysis (34.3±1.4%) and HONO photolysis (18±2.5%). On the other hand, while the reaction between OH and NO₂ served as the sole sink of RO_x at TC, it only explained 50% of RO_x sink at WS with the other half attributable to self-consumption of peroxy radicals.

For details, please refer to Section 3.3.3 in the revised manuscript.

14. Page 21, Lines 15-22: it is surprising that the O₃ production rates at WS were much higher than those at TC, especially on the episode days, given that the NO_x and VOC

levels were much higher at TC than at WS during O₃ episodes. What's the possible reason for this?

Thanks for the comment and question. With the addition of HONO in O₃ simulation, the new modeling results show that the net O₃ production rate at WS was comparable to that at TC during non-episodes. However, it was much higher than that at TC during O₃ episodes, due to the more abundant peroxy radicals (RO₂ and HO₂) at WS, in addition to the increased NO during O₃ episodes which unleashed the potential of O₃ production through the reactions between peroxy radicals and NO. It should be noted that the increase of NO at WS during O₃ episodes did not lead to O₃ reduction, unlike the situation in most urban environments including TC, because O₃ formation at WS was limited by both VOCs and NO_x and more sensitive to NO_x without the input of continental air. Overall, despite the lower VOCs and NO_x, the concentrations of peroxy radicals at WS were higher than at TC (the reasons have been discussed in responses to comment #13), and the increase of NO during O₃ episodes accelerated O₃ formation through the reactions between peroxy radicals and NO.

Furthermore, the production and loss rates of O₃ were simulated (Figure 5(b)). Despite the increased O₃ mixing ratio during episodes (Table 3), there was no significant change in net O₃ production between O₃ episodes (2.5 ± 1.0 ppbv/h) and non-episodes (2.5 ± 0.5 ppbv/h) at TC ($p > 0.05$), suggesting that regional transport might play critical roles in regulating O₃ levels at TC. In fact, previous studies (Huang et al., 2006; Jiang et al., 2008) have repeatedly confirmed that O₃ pollution at this site could be aggravated under northerly winds and/or downdraft on the periphery of typhoon. In contrast, the net O₃ production increased remarkably from non-episodes (2.8 ± 0.5 ppbv/h) to O₃ episodes (6.6 ± 1.1 ppbv/h) at WS. Obviously, O₃ production at WS was much higher than at TC during O₃ episodes, while they were comparable during non-episodes. This was likely due to the more abundant peroxy radicals (RO₂ and HO₂) at WS than at TC, in addition to the increased NO_x during O₃ episodes which enhanced the reactions between the peroxy radicals and NO (increasing O₃ formation). Insight into the O₃ production pathways found that the reaction rates of RO₂+NO and HO₂+NO were significantly enhanced from 1.6 ± 0.2 and 2.0 ± 0.4 ppbv/h during non-episodes to 3.2 ± 0.5 and 5.2 ± 0.9 ppbv/h during O₃ episodes, respectively. Our recent study (Wang et al., 2017b) revealed that O₃ formation at WS was in a

transition regime and much more sensitive to NO_x during non-episodes, when O_3 production through peroxy radicals reacting with NO was seriously limited by the low NO_x . During O_3 episodes, with the increase O_3 precursors (particularly NO_x), these reactions were accelerated and the net O_3 production increased substantially. Detailed discussion on the O_3 photochemistry at WS can be found in our recent publication (Wang et al., 2017b).

For details, please refer to Section 3.3.3 in the revised manuscript.

15. Section 3.3.3 and Figure 5: it would be better if the ozone production rates were expressed in ppb/h so that it can be easily compared with the observed ozone increase.

The good suggestion has been accepted with thanks.

1 **Ozone pollution around a coastal region of South China Sea: Interaction between marine and**
2 **continental air**

3 Hao Wang^{1#}, Xiaopu Lyu^{1#}, Hai Guo^{*.1}, Yu Wang¹, Shichun Zou², Zhenhao Ling³, Xinming
4 Wang⁴, Fei Jiang^{**5}, Yangzong Zeren¹, Wenzhuo Pan¹, Xiaobo Huang⁶, Jin Shen⁷

5 ¹ Air Quality Studies, Department of Civil and Environmental Engineering, Hong Kong
6 Polytechnic University, Hong Kong, **China**

7 ² School of Marine Sciences, Sun Yat-sen University, China

8 ³ School of Atmospheric Sciences, Sun Yat-sen University, China

9 ⁴ Guangzhou Institute of Geochemistry, Chinese Academy of Sciences, Guangzhou, China

10 ⁵ International Institute for Earth System Science, Nanjing University, China

11 ⁶ Shenzhen Academy of Environmental Sciences, Shenzhen, China

12 ⁷ State Key Laboratory of Regional Air Quality Monitoring, Guangdong Key Laboratory of
13 Secondary Air Pollution Research, Guangdong Environmental Monitoring Center, Guangzhou,
14 China

15
16 *Corresponding to:* * H. Guo (ceguohai@polyu.edu.hk) and ** F. Jiang (jiangf@nju.edu.cn)

17 [#]These authors contributed equally to this work.

18

1 **Abstract**

2 Marine atmosphere is usually considered to be a clean environment, while this study indicates
3 that the near-coast waters of South China Sea (SCS) suffered from even worse air quality than
4 coastal cities. The analyses were based on concurrent field measurements of target air pollutants
5 and meteorological parameters conducted at a suburban site (**Tung Chung, TC**) and a nearby
6 marine site (**Wan Shan, WS**) from August to November 2013. The observations showed that the
7 levels of primary air pollutants were significantly lower at WS than those at TC, while ozone (O₃)
8 value was greater at WS. Higher O₃ levels at WS were attributed to the weaker NO titration and
9 higher O₃ production rate because of stronger oxidative capacity of the atmosphere. However, O₃
10 episodes were concurrently observed at both sites under certain meteorological conditions, such
11 as tropical cyclones, continental anticyclones and sea-land breezes (SLBs). Driven by these
12 synoptic systems and mesoscale recirculations, the interaction between continental and marine
13 air masses had profoundly changed the atmospheric composition and subsequently influenced
14 the formation and redistribution of O₃ in the coastal areas. When continental air intruded into
15 marine atmosphere, the O₃ pollution was magnified over SCS, and the elevated O₃ (>100 ppbv)
16 could overspread the sea boundary layer ~8 times the area of Hong Kong. In some cases, the
17 exaggerated O₃ pollution over the SCS was re-circulated to the coastal inshore by sea breeze,
18 leading to even aggravating O₃ pollution in coastal cities. The findings are applicable to similar
19 mesoscale environments around the world where the maritime atmosphere is potentially
20 influenced by severe continental air pollution.

21 **Key words:** Continental air pollution; Maritime atmosphere; Mesoscale recirculation; Ozone
22 photochemistry

23

24

1 **1 Introduction**

2 Ozone (O₃) plays a central role in photochemical oxidation processes in the troposphere via
3 direct reaction, photolysis and the subsequent reactions to produce the hydroxyl radical (Monks
4 et al., 2015; Seinfeld and Pandis, 2016). As a strong oxidant, O₃ at surface level is recognized to
5 be a threat to human health (WHO, 2003; Bell et al., 2007) and has a detrimental impact on
6 vegetation (Fowler et al., 2009) and built infrastructure (Kumar and Imam, 2013). Tropospheric
7 O₃ is also the third most important greenhouse gas (IPCC, 2014) and is referred to a short-lived
8 climate pollutant (Shindell et al., 2012).

9 To mitigate O₃ pollution in the troposphere, tremendous efforts from both scientific and
10 regulatory communities have been made since three decades ago (NRC, 1991; NARSTO, 2000;
11 Monks et al., 2015). The O₃ levels started to decrease at many locations, such as Jungfrauoch in
12 Switzerland, Zugspitze in Germany, Mace Head in Ireland, as well as parts of California and
13 eastern US (Lefohn et al., 2010; Cui et al., 2011; Parrish et al., 2012; Lin et al., 2017). However,
14 increasing studies showed that surface O₃ was elevated rapidly in East Asia in the last decade
15 (Ding et al., 2008; Xu et al., 2008; Parrish et al., 2012; Xue et al., 2014; Zhang et al., 2014; Sun
16 et al., 2016; Lin et al., 2017; Wang et al., 2017a). For example, the observational data revealed
17 that regional O₃ concentrations increased at a rate of 0.86 ppbv yr⁻¹ in Pearl River Delta (PRD)
18 from 2006 to 2011 (Li et al., 2014), at a rate of 0.56 ppbv yr⁻¹ in Hong Kong from 2005 to 2014
19 (Wang et al., 2017a), and even at a rate of 1.7-2.1 ppbv yr⁻¹ (summertime only) at Mount Tai in
20 central eastern China (Sun et al., 2016).

21 Hong Kong and the adjacent PRD is the most industrialized region along the coast of South
22 China Sea (SCS), and is suffering from serious O₃ pollution (Zheng et al., 2010; Derwent et al.,
23 2013; Ling et al., 2013). Numerous studies demonstrated that in addition to long-range transport
24 (Chan, 2002; Guo et al., 2009; Wang et al., 2009) and local photochemical production (Ding et
25 al., 2013a), tropical cyclones and mesoscale circulations are conducive to the occurrence of high
26 O₃ events (Yin, 2004; Huang et al., 2005; Yang et al., 2012; Jiang et al., 2015; Wei et al., 2016).
27 In a number of studies, tropical cyclone has been considered as the most conducive driver to the
28 occurrence of O₃ episodes in Hong Kong (Yin, 2004; Ling et al., 2013) for it generally causes

1 peripheral subsidence, stagnation air and inversion layer, which favor the production and
2 accumulation of O₃.

3 Mesoscale circulations (*e.g.*, sea-land breezes (SLB) and mountain–valley breezes) also play
4 important roles in O₃ distribution and transport in the coastal cities like Hong Kong with
5 complex topography and land cover (Liu and Chan, 2002; Ding et al., 2004; Lu et al., 2009a;
6 Guo et al., 2013). For instance, Guo et al. (2013) demonstrated that upslope winds brought
7 pollutants including O₃ from low-lying areas to the peak of Mt Tai Mo Shan (957 m a.s.l.) in
8 Hong Kong. Ding et al. (2004) simulated a multi-day SLB related O₃ episode and discussed the
9 influence of SLB circulation on the transport of oxidant precursors, the residence time and re-
10 entry of photochemical compounds. Lu et al. (2010) simulated the SLB in the 2003/2004 winter
11 and revealed that the urbanization of Shenzhen might significantly enhance the sea breeze to the
12 west of Hong Kong in the early afternoon, which worsened the local air pollution.

13 Both coastal human activities and marine atmospheric cyclic behavior can significantly affect the
14 air pollution level in coastal urban environments (Adame et al., 2010; Velchev et al., 2011).
15 Exploring SLBs provides an important way to understand the interaction between continental air
16 and marine atmosphere which has long been a focus of coastal air quality, global tropospheric
17 chemistry and climate change research. Surprisingly, few studies investigated SLBs in Hong
18 Kong though about 70 SLB days per year on average were observed in Hong Kong and the PRD
19 region (Zhang and Zhang, 1997). Therefore, the association between mesoscale recirculation and
20 air pollutants over the SCS and subtropical continental region is still not well established, which
21 seriously limits our understanding on the interplay of continental and marine air masses in this
22 region. Furthermore, previous O₃ studies carried out in this region neither paid enough attention
23 to the variations of volatile organic compounds (VOCs, one important group of O₃ precursors)
24 nor established any field measurements on an island, an ideal site for observation of marine air
25 mass with less interference from local emissions, for understanding the O₃ pollution around the
26 coastal region of the SCS (Parrish et al., 1998). So far, only a handful of studies deeply evaluated
27 the chemical characteristics of air masses under various synoptic systems (Wang et al., 2005;
28 Guo et al., 2009, 2013; [Li et al., 2018](#)).

1 This study aimed to comprehensively characterize interaction between continental anthropogenic
2 emissions and marine atmosphere over a coastal region of the SCS by concurrent measurements
3 and in-depth analysis of air pollutants at a marine site over SCS and a suburban site in Hong
4 Kong. Firstly, the spatial and temporal variations of measurements were described to give an
5 overall picture of the campaign, as well as to directly evaluate how continental outflows polluted
6 the marine atmosphere over the SCS. After that, the chemical and meteorological characteristics
7 of air masses associated with high O₃ concentrations were explored. Finally, the interplay
8 between the maritime and continental air masses and its influence on regional air quality were
9 discussed.

10 **2 Methodology**

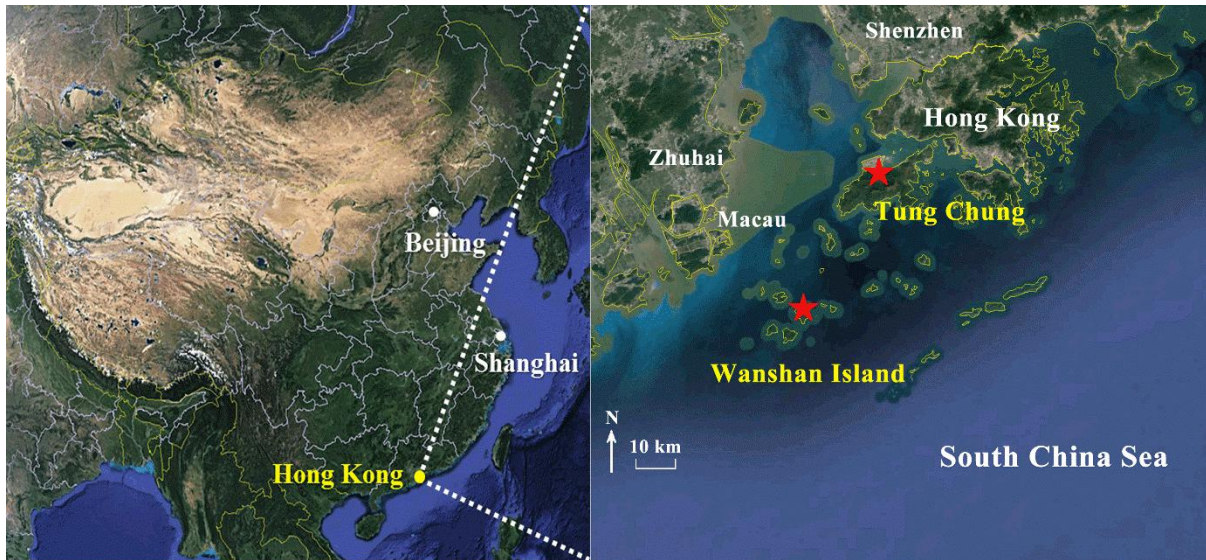
11 **2.1 Sampling sites**

12 Field measurements were carried out concurrently at a suburban site and a marine site over SCS
13 (Figure 1). The suburban Tung Chung (TC, 22.29 ° N, 113.94 ° E) site, part of the Hong Kong
14 Environmental Protection Department (HKEPD) air quality monitoring network, is located in
15 southwestern Hong Kong, about 3 km south of the Hong Kong International Airport at Chek Lap
16 Kok with Hong Kong urban center about 20 km to the southwest and Macau 38 km to the
17 northeast. It is a newly-developed residential town adjacent to the busy highway and railway
18 lines. The sampling instruments were installed on the rooftop of a building with a height of 27.5
19 m a.s.l. More detailed description of the TC site can be found in our previous publications
20 (Cheng et al., 2010a; Jiang et al., 2010).

21 The marine site, Wan Shan island (WS, 21.93 ° N, 113.73 ° E), is located 40 km southeast of
22 Zhuhai, and is bounded to the north by the Pearl River Estuary, with a straight distance of about
23 44 km to TC. WS has an area of 8.1 km² and a population of about 3,000 with sparse
24 anthropogenic emissions at the island. The isolated island features a sub-tropical maritime
25 climate. The measurement site was set up on the rooftop of the National Marine Environmental
26 Monitoring Station with a height of about 65 m a.s.l.

27 High O₃ mixing ratios are frequently observed in Hong Kong in late summer and autumn (Ling
28 et al., 2013) when **tropical cyclones** and the northeast monsoon prevail, **respectively**. During this

1 period, WS is right in the downwind direction of TC, which facilitates the study of the
2 interaction between the inland pollution and the marine environment.



3
4 **Figure 1.** Locations of the sampling sites (red stars) and the surrounding environment.
5

6 **2.2 Measurement techniques**

7 *2.2.1 Measurements of trace gases and meteorological parameters*

8 The sampling campaign was conducted from 10 Aug. to 21 Nov. across late summer and autumn
9 in 2013. At WS, trace gases (*i.e.*, NO_x , O_3 , SO_2 and CO) were continuously monitored with a time
10 resolution of 1 minute. $\text{NO-NO}_2\text{-NO}_x$ was measured using a heated molybdenum NO_2 -to- NO
11 converter and a chemiluminescence analyzer (*Thermo Environmental Instruments (TEI), Model*
12 *42i*) with a range of 0-200 ppbv and a lower detection limit of 0.40 ppbv. It was noteworthy
13 that the measured NO_x might include other oxidized reactive nitrogen that was converted by the
14 molybdenum. Thus, the NO_x concentrations given below were considered the upper limits of
15 their actual values (Dunlea et al., 2007; Ran et al., 2011). O_3 was monitored with a commercial
16 UV photometric analyzer (*TEI, Model 49i*) with a range of 0-0.050 to 200 ppm and a lower
17 detection limit of 1.0 ppbv. SO_2 was measured using a pulsed UV fluorescence approach (*TEI,*
18 *Model 43S*). CO was measured by a gas filter correlation, non-dispersive infrared analyzer (*API,*
19 *Model 300*) with a heated catalytic scrubber to convert CO to CO_2 for baseline determination.

1 Quality assurance and control procedures (*e.g.*, instrumental maintenance and calibration) for
2 these devices have been described elsewhere (Guo et al., 2009, 2013). Meteorological
3 parameters, including temperature, relative humidity, solar radiation, wind speed and wind
4 direction, were routinely monitored by a weather station (Vantage Pro 2 plus, Davis Instruments)
5 with a time resolution of 5 minutes. At TC, hourly data of the aforementioned trace gases and
6 meteorological parameters were obtained from the HKEPD
7 (<http://epic.epd.gov.hk/ca/uid/airdata>). Detailed information of the quality assurance and control
8 protocols is available in the HKEPD report (HKEPD, 2015).

9 *2.2.2 Sampling and analysis of VOCs*

10 Concurrent VOC samples (*i.e.*, non-methane hydrocarbons (NMHCs) and carbonyls) were
11 collected on 21 selected days (including both non-O₃ episodes and O₃ episodes) at both sites.
12 These days were selected on the basis of weather prediction and meteorological data analysis for
13 potentially high and low O₃ days. An O₃ episode day is the day when the peak one-hour averaged
14 O₃ mixing ratio exceeds 100 ppbv (Level II of China National Ambient Air Quality Standard).
15 Please refer to our previous publication for details of this method (Guo et al., 2009).

16 The whole-air samples of NMHCs were collected using 2-L electro-polished stainless steel
17 canisters. The canisters were cleaned, conditioned and evacuated before being used for
18 sampling. A metal bellows pump was used to fill up the canisters with sample air over one-hour
19 integration (with a flow restrictor) to a pressure of 40 psi. Seven one-hour VOC samples (every
20 two hours during 7:00 – 19:00 inclusive) were collected simultaneously at each site. Intensive
21 VOC sampling was also carried out at WS in selected seven days (*i.e.*, 3, 4, 9 and 22-25 October) with
22 eleven one-hour samples (every two hours during 1:00 – 22:00 inclusive). Totally, 311 valid
23 VOC samples (144 at TC and 167 at WS) were collected in addition to about 5% field blanks and
24 5% parallel samples for quality assurance purpose. The speciation and abundance of 59 C₂-C₁₁
25 NMHCs in the canisters were determined by a Model 7100 preconcentrator (Entech Instruments
26 Inc., California, USA) coupled with an Agilent 5973N gas chromatography-mass selective
27 detector/flame ionization detector (GC-MSD/FID, Agilent Technologies, USA). The detection
28 limit of NMHCs was 3 pptv with a measurement precision of 2-5%, and a measurement accuracy

1 of 5%. Detailed information of the analysis system and quality control and quality assurance for
2 VOC samples can be found elsewhere (Simpson et al., 2010).

3 Carbonyl samples were collected using silica gel filled cartridges impregnated with acidified 2,4-
4 dinitrophenylhydrazine (DNPH). Air samples were drawn through the cartridge at a flow rate of
5 0.8–0.9 L min⁻¹ for 2 hours; the flow rate through the cartridges was monitored with a rotameter
6 which was calibrated before and after each sampling. An O₃ scrubber was connected to the inlet
7 of the DNPH–silica gel cartridge to prevent interference from O₃. In total, 227 carbonyl samples
8 (124 at TC and 103 at WS) were collected with 5 and 6 samples per non-O₃ and O₃ episode day
9 (every two hours during 7:00 - 18:00 inclusive), respectively. All cartridges were stored in a
10 refrigerator at 4 °C after sampling. The sampled carbonyl cartridges were eluted slowly with <5
11 ml of acetonitrile in the direction opposite to sampling flow into a 5-ml brown volumetric flask,
12 followed by adding acetonitrile to a constant volume of 5 ml. A 20- μ l aliquot was injected into
13 the high performance liquid chromatography (HPLC) system through an auto-sampler. The
14 operating conditions of the HPLC are shown in Table S1. Typically, C₁–C₉ carbonyl compounds
15 were measured efficiently with a detection limit of ~0.2 ppbv.

16 **2.3 Observation-based model (OBM)**

17 A photochemical box model coupled with the Master Chemical Mechanism v3.2 (PBM-MCM)
18 was applied to simulate the O₃ production at WS and TC for the VOC sampling days. The PBM-
19 MCM model is a zero-dimension photochemical box model combined with a near explicit
20 chemical mechanism consisting of 5,900 species and 16,500 reactions, which fully describes the
21 mechanisms of homogeneous reactions in the atmosphere (Jenkin et al., 1997; Jenkin et al., 2003;
22 Saunders et al., 2003). The simulation was constrained by hourly data of meteorological
23 parameters (*i.e.*, temperature and relative humidity) and air pollutants (NO, NO₂, CO, SO₂ and
24 51 measured VOCs). Since the sampling interval was two hours for each sample, cubic spline
25 interpolation was used to derive VOC concentrations at each hour for modeling purpose. Please
26 see our previous publication for details (Wang et al., 2017a). **HONO has been recognized as an**
27 **important source of OH, influencing O₃ formation significantly (Kleffmann, 2007). Since we did**
28 **not measure HONO mixing ratios in this study, the average diurnal profiles of HONO observed**
29 **at TC in autumn 2011 (Xu et al., 2015) and at a coastal background site (Hok Tsui, HT) in**
30 **southeast Hong Kong in autumn 2012 (Zha, 2015) were applied to the photochemical**

1 simulations at TC and WS, respectively. Figure S1 shows the average diurnal cycles of HONO at
2 TC and HT. The use of the aforementioned diurnal profiles might increase the uncertainty of
3 model simulation. However, we believe that the newly introduced uncertainties could not be too
4 high, because HONO observations at TC and HT were carried out 2 years and 1 year before the
5 sampling campaign of this study, respectively. In addition, HT was comparable to WS in aspects
6 of local emissions (nearly free of anthropogenic emissions), air mass category (mixed continental
7 and marine air) and location (to the south of Hong Kong and on SCS). It is noteworthy that the
8 atmospheric physical processes (*i.e.*, vertical and horizontal transport) were not considered in
9 this model. In addition, the inherent uncertainty of NO_x measurement mentioned above might
10 slightly affect the modeling results. The PBM-MCM model has been successfully applied in
11 previous studies (Cheng et al., 2010b; Lam et al., 2013; Ling et al., 2014). Details of the model
12 construction can be found in Saunders et al. (2003) and Lam et al. (2013).

13 **2.4 WRF-CMAQ simulation and backward particle release model**

14 In this study, the Weather Research and Forecasting (WRF v3.7.1) model (Skamarock et al.,
15 2008) was used to simulate vertical and horizontal wind fields for various weather systems
16 observed in this campaign, and then provided meteorological parameters required by U.S. EPA
17 Community Multiscale Air Quality (CMAQ v4.7.1) model (www.epa.gov/cmaq). CMAQ is a
18 three-dimensional Eulerian atmospheric chemistry and transport modeling system, which
19 includes complex physical and chemical processes, such as physical transport and diffuse, gas
20 and aqueous chemical transformation, and so on; and it can treat multiple pollutants
21 simultaneously from local to continental scales. A domain system composed of four
22 nested grids (81, 27, 9, 3 km) was adopted to better suit the simulation of mesoscale weather
23 systems, as shown in Figure S2. The domain with finest resolution (3 km) covers the Pearl River
24 Estuary region. Vertically, there were 31 sigma levels for all domains, with the model top fixed
25 at 50 hPa. The major selected physical schemes invoked in WRF and chemical mechanisms used
26 in CMAQ are shown in Table S2. The input meteorological data was made using NCEP FNL
27 (final) data with a horizontal resolution of 1°×1° (<https://rda.ucar.edu/>). In addition, the
28 geographical data were obtained from the Research Data Archive of National Center for
29 Atmospheric Research (NCAR) (<http://www2.mmm.ucar.edu/wrf/users/downloads.html>). The
30 emission inventories (EI) used in this study included the 2000-based Regional Emission

1 Inventory in ASia (REAS) (Kurokawa et al., 2013) and the 2010-based Multi-resolution
2 Emission Inventory for China (MEIC) (He, 2012), both of which were processed by the Sparse
3 Matrix Operating Kernel Emission (SMOKE) model. The biogenic emissions were calculated by
4 the Model of Emissions of Gases and Aerosols from Nature (MEGAN) (Guenther, 2006). The
5 WRF modelling mainly focused on O₃ episodes with an additional 24hrs' preceding run as spin-
6 up for each episode, and the integration was conducted separately. In addition, the
7 spatiotemporal patterns of CO and O₃ were simulated by WRF-CMAQ during two O₃ episodes
8 (see section 3.4). **The time series of the simulations and observations of CO and O₃ are shown in**
9 **Figure S3. Also,** Table S3 gives the index of agreements (IOAs) between the simulated and
10 observed meteorological parameters and air pollutants. Within the range of 0 – 1, higher IOAs
11 represent better agreement between the simulated and observed values (Willmott, 1982). Here,
12 IOA was between 0.51 and 0.84 for the simulation of meteorological parameters. Furthermore, it
13 was not lower than 0.50 for primary air pollutants, and reached 0.81 for O₃ simulation at both
14 sites. The model performances were comparable to those reported in previous studies (Cabaraban
15 et al., 2013; Wang et al., 2015). Therefore, we accepted the modeling results, in view of the fact
16 that the simulations were only used to qualitatively indicate the interactions between the
17 continental and marine air in this study.

18 Backward particle release simulations were carried out using HYSPLIT model (Stein et al., 2015)
19 for episode days at WS and TC sites during the entire sampling period (Draxler and Rolph, 2003).
20 The backward particle release simulation, which considers the dispersion processes in the
21 atmosphere, is capable of identifying the history of air masses (Guo et al., 2009; Ding et al.,
22 2013a, 2013b). In this work, we applied the model following a method developed by Ding et al.
23 (2013a).

24 **3 Results and Discussion**

25 **3.1 Spatio-temporal variations**

26 Table 1 summarizes the meteorological conditions and chemical species observed at WS and TC.
27 Lower temperature ($25.7 \pm 0.1^\circ\text{C}$) and higher relative humidity ($82.8 \pm 0.4\%$) were recorded at the
28 marine site (WS) compared to the suburban site (TC) ($p < 0.01$) (temperature: $26.7 \pm 0.1^\circ\text{C}$ and
29 relative humidity: $67.7 \pm 0.5\%$). At WS, the solar radiation ($635.8 \pm 46.9 \text{ Wm}^{-2}$) was much higher
30 than that at TC ($563.5 \pm 46.1 \text{ Wm}^{-2}$, $p < 0.01$), while the average wind speed at TC ($4.6 \pm 0.1 \text{ ms}^{-1}$)

1 was significantly lower than that measured at WS ($7.2 \pm 0.2 \text{ms}^{-1}$). The lower wind speed at TC
 2 was related to the roughness of underlying surfaces. However, no statistical differences were
 3 found for the average wind direction (about 81° , northeast wind) at the two sites, indicating that
 4 the two sites were probably under the influence of similar air masses in most cases.

5 The NO, NO₂, CO, SO₂ and total VOCs (the sum of NMHCs and carbonyls) had lower average
 6 and maximum mixing ratios at WS than those at TC. The lower levels of primary air pollutants at
 7 WS were likely the results of fewer local emission sources, faster photochemical consumption
 8 (as discussed later) and/or more favorable dispersion conditions (*e.g.*, higher wind speed). In
 9 contrast, O₃ was much higher at WS (Table 1), attributable to the enhancements by both
 10 meteorological and photochemical effects, as discussed in sections 3.2 and 3.3.

11 **Table 1.** Descriptive statistics of meteorological parameters and trace gases at the two sites
 12 during the sampling period.

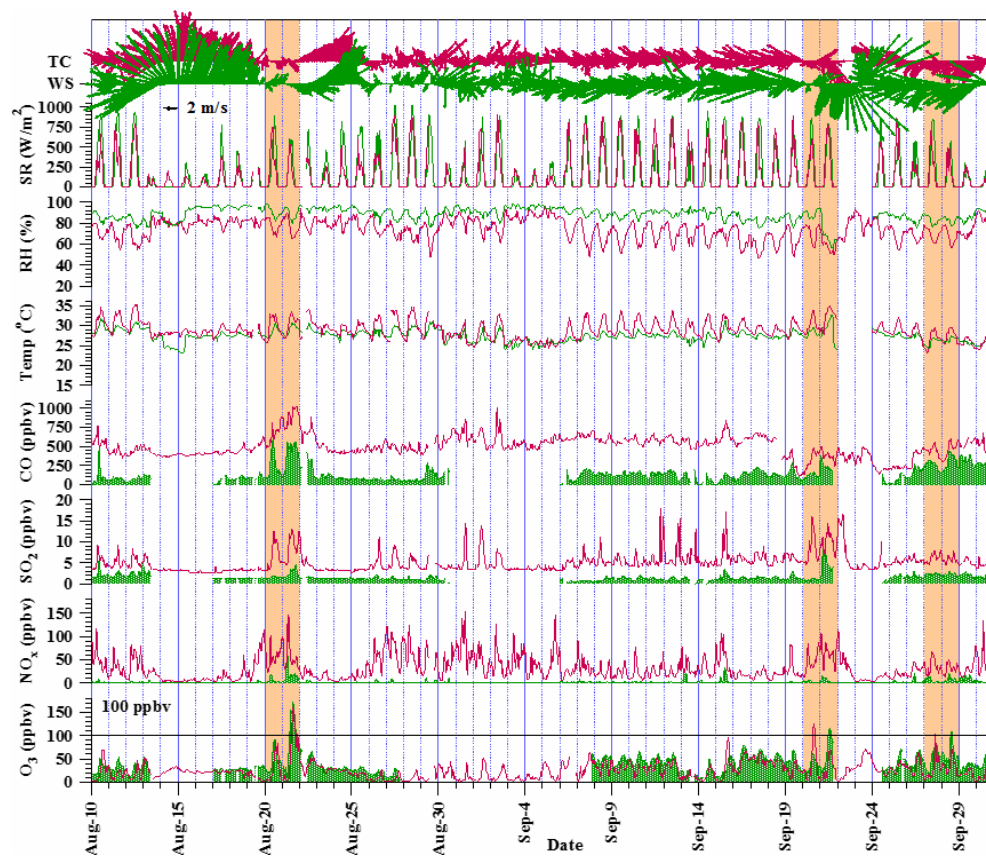
Parameter	WS		TC	
	<i>Mean ± 95% C.I.</i>	<i>Max.</i>	<i>Mean ± 95% C.I.</i>	<i>Max.</i>
Temperature (°C)	25.7 ± 0.1	32.8	26.7 ± 0.1	35.4
Relative humidity (%)	82.8 ± 0.4	98.9	67.7 ± 0.5	96.8
Solar radiation (W m ⁻²)*	635.8 ± 46.9	1026.8	563.5 ± 46.1	910.0
Wind speed (m s ⁻¹)	7.2 ± 0.2	23.8	4.6 ± 0.1	13.8
Wind direction (°)	81.3	-	80.9	-
O ₃ (ppbv)	51.3 ± 1.2	173.0	30.0 ± 1.0	159.9
NO (ppbv)	0.7 ± 0.1	21.0	14.0 ± 0.8	115.7
NO ₂ (ppbv)	4.3 ± 0.3	49.3	25.0 ± 0.6	104.2
CO (ppbv)	251.4 ± 6.5	727.7	560.5 ± 6.3	1047.9
SO ₂ (ppbv)	2.4 ± 0.1	12.2	5.9 ± 0.1	19.1
NMHCs (ppbv)	12.7 ± 1.1	32.9	17.7 ± 1.7	60.0

Carbonyls (ppbv)	7.9±0.7	16.3	9.2±0.7	26.5
------------------	---------	------	---------	------

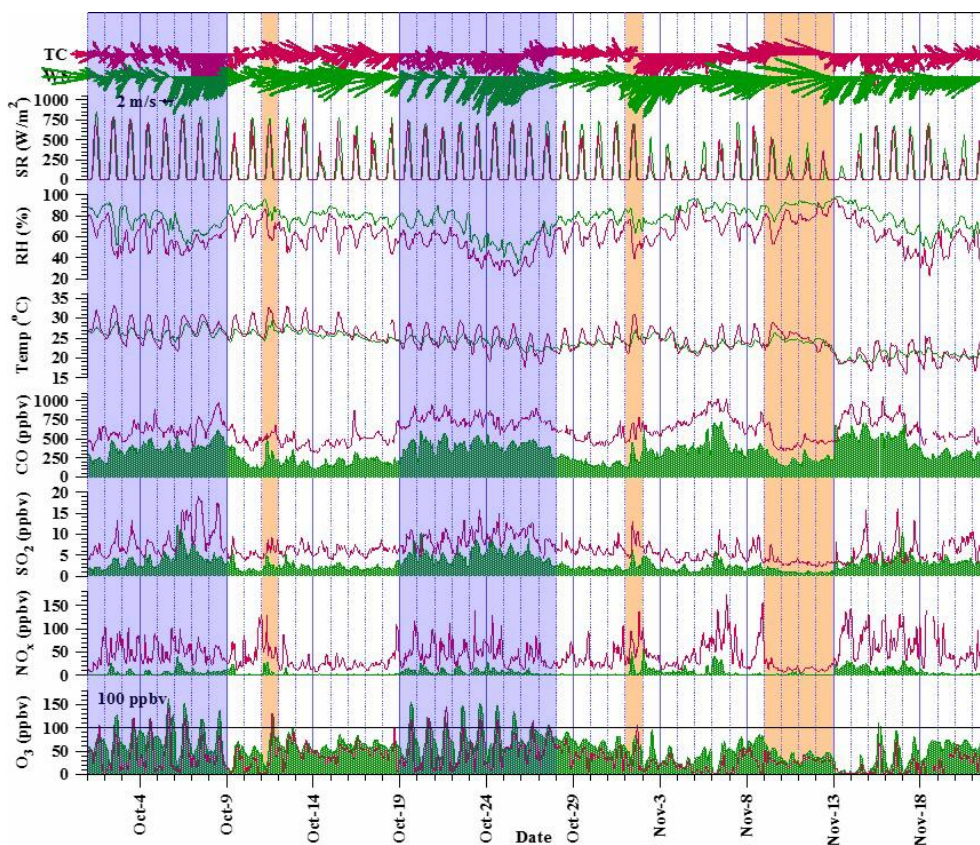
* Average of the daily maximum solar radiation. *C.I.* denotes confidence interval.

Time series of local meteorological parameters and hourly mixing ratios of air pollutants at the two sites are illustrated in Figures 2a-2b. The temporal patterns of wind directions were generally similar at both sites, with the dominance of the southerly winds in August and northeastern winds between September and November. Occasionally, the northwesterly winds from the PRD region were observed.

This sampling campaign witnessed 17 O₃ episodes and 7 near-O₃ episode days at TC, which refers to the days with maximum hourly mixing ratio of O₃ higher than 100 ppbv and within the range of 80-100 ppbv, respectively. (80 ppbv was Level I of China National Ambient Air Quality Standard for O₃). At WS, 21 O₃ episodes and 6 near-O₃ episodes were recorded. Specifically, 13 O₃ episode days were simultaneously observed at the two sites, with the rest occurred exclusively at one site. On one hand, the primary air pollutants (CO, SO₂ and NO_x) generally increased during O₃ episodes, implying enhanced O₃ formation potentials from the precursors. On the other hand, O₃ episodes were always accompanied by the synoptic conditions, *i.e.*, tropical cyclone (typhoon in the mature form) and continental anticyclone, and/or mesoscale circulations such as SLB, as detailed in Table S4. For example, the two multi-day O₃ episode events, *i.e.*, 1-8 Oct. and 19-27 Oct. (highlighted in blue in Figure 2), were strongly associated with continental high pressure. These episode days generally had high temperature, northerly winds, and intensive solar radiation, with air flows largely from the inland or the coastal areas. Also, the mixing ratios of CO, NO₂ and SO₂ usually increased during these days, suggesting the accumulation of local air pollutants and/or the increasing contribution from regional transport. In contrast, O₃ episodes under the influence of tropical cyclones (highlighted in orange in Figure 2) featured high temperature, strong solar radiation and typically calm or moderate northwesterly to northeasterly winds, except for typhoon “Haiyan” occurred on 9-12 Nov. (discussed in section 3.2.1). These conditions were all conducive to the formation and accumulation of O₃. Additionally, SLB was also an important factor regulating O₃ pollution in this region during O₃ episodes (Table S4). Detailed discussions can be found in section 3.2.3.



1
 2 **Figure 2a.** Time series of trace gases and meteorological parameters observed for the sampling
 3 period of 10 Aug. - 30 Sept. at WS (green) and TC (red). The black line of 100 ppbv is the
 4 threshold for O₃ episode definition. The dates seriously affected by continental high pressure and
 5 tropical cyclones are shaded in blue and orange, respectively. Note that there are some data
 6 missing in these months due to extremely bad weather conditions and instrumental failure.
 7



1
 2 **Figure 2b.** Time series of trace gases and meteorological parameters observed for the sampling
 3 period of 1 Oct. - 21 Nov at WS (green) and TC (red). The black line of 100 ppbv is the
 4 threshold for O₃ episode definition. The dates seriously affected by continental high pressure
 5 and tropical cyclones are shaded in red and orange, respectively.

6
 7 **3.2 Meteorological influence on O₃ mixing ratios**

8 Descriptive statistics of meteorological parameters during O₃ episode and non-episode days are
 9 summarized in Table 2. On episode days the wind speed and relative humidity were lower
 10 whereas solar radiation was stronger at both sites, suggesting that this type of weather condition
 11 was conducive to the formation and accumulation of tropospheric O₃. Furthermore, the wind
 12 direction during non-episodes was predominantly from the east (SCS), while on episodes the
 13 winds mainly came from the north and northeast which might bring more pollutants from the
 14 urban areas of Hong Kong and inland PRD to the sampling sites. The characteristics of O₃
 15 pollution under different weather conditions were discussed below.

1
 2 **Table 2.** Descriptive statistics (Mean±95% C.I.) of meteorological parameters at the two sites
 3 during O₃ episodes and non-O₃ episodes days.

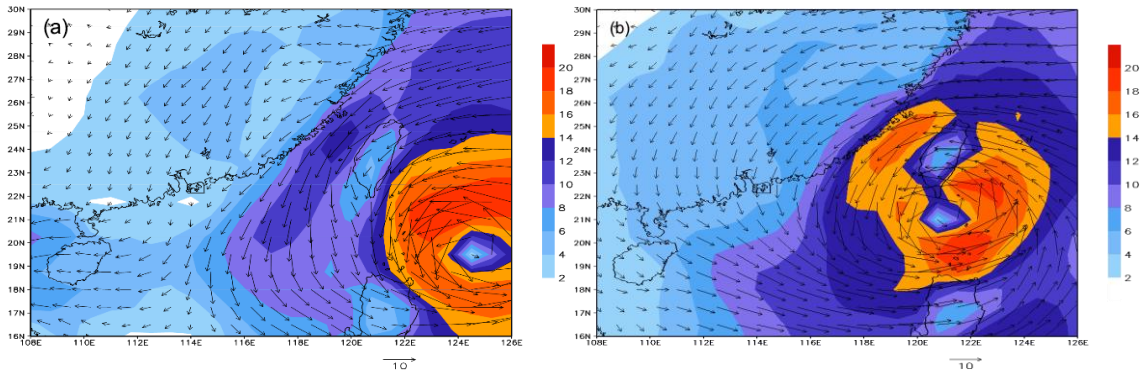
Parameter	WS		TC	
	<i>O₃ episode</i>	<i>Non-O₃ episode</i>	<i>O₃ episode</i>	<i>Non-O₃ episode</i>
Temperature (°C)	25.3±0.2	25.8±0.1	26.3±0.3	26.8±0.2
Wind speed (m s⁻¹)	5.3±0.2	7.7±0.2	3.7±0.2	4.8±0.1
Wind direction (°)	45.1	89.1	19.5	86.8
Relative humidity (%)	71.7±1.2	85.7±0.4	58.4±1.4	69.6±0.6
Solar radiation (W m⁻²)*	723.2±26.1	613.7±57.6	699.0±29.1	537.0±53.1

4 * Average of the daily maximum solar radiation. *C.I.* denotes confidence interval.

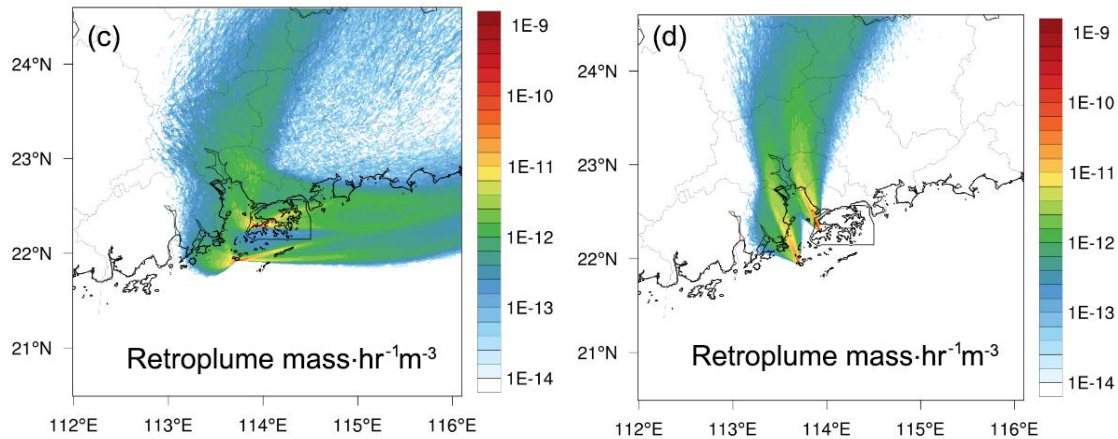
5
 6 *3.2.1 Tropical cyclones*
 7 Tropical cyclone (low-pressure system) is one of the main meteorological conditions conducive
 8 to the occurrence of O₃ episodes in Hong Kong (Yin, 2004; Ling et al., 2013). In this study, 7
 9 episode days and 3 near-episode days were closely associated with 5 tropical cyclones (*i.e.*,
 10 Trami, Usagi, Wutip, Nari and Krosa) (Table S4 and Figure S4). For example, Trami caused the
 11 worst O₃ episode on 21 Aug. with the highest peak hourly O₃ mixing ratios of 160 and 173 ppbv
 12 at TC and WS, respectively. These episode or near-episode days usually appeared 1-2 days
 13 before the arrival of the tropical cyclones, because the large-scale peripheral subsidence of the
 14 tropical cyclones usually creates the meteorological conditions favorable to the formation and
 15 accumulation of O₃, such as inversion layer, high temperature, low humidity, intensive light, and
 16 weak winds (Wang et al., 1998; Yin, 2004). The tropical cyclones also cause anti-clockwise air
 17 flows at their outskirt affecting the wind directions and subsequent the regional transport of air
 18 pollution. Figure 3 illustrates surface wind fields and air movement two days (*i.e.*, 20-21 Sept.)
 19 before the occurrence of Usagi as an example. It can be seen that when Usagi approached
 20 southeastern area of Hong Kong, it led to weak northeasterly and later northwesterly winds
 21 which potentially delivered O₃ and its precursors from highly polluted inland PRD region to the

1 sampling sites (Yin, 2004; Wei et al., 2016; Wang et al., 2017a). The wind speed was lower than
2 4 m s^{-1} at the sampling sites and in their surrounding area on 20 Sept. (Figure 3a), and it
3 gradually increased on the next day (21 Sept.) with the approaching of the tropical cyclone
4 (Figure 3b). It is noteworthy that the rarely occurred westerly and northwesterly winds caused
5 tropical cyclones resulted in unsynchronized occurrence of O_3 episodes between the two sites
6 (Figures 3c & d). Namely, high O_3 values were observed at TC only on 20 Sept., while O_3 started
7 to increase at WS on the next day (21 Sept.). This discrepancy might indicate the transport of O_3
8 and/or its precursors from terrestrial area to the offshore site driven by tropical cyclone.

9 Please note, not all tropical cyclones would cause high levels of O_3 . For example, the tropical
10 cyclone Haiyan observed on 9-12 Nov. over the SCS did not cause high O_3 levels (Figure 2b).
11 Because the origin of Haiyan was at a lower latitude (southern Guam) and it moved on the
12 waters southwest of PRD (Figure S4), the anti-clockwise air flow caused easterly and
13 southeasterly winds in the north and northeast outer band of Haiyan. The winds originated from
14 SCS brought in clean marine air to the sampling sites, resulting in dilution and dispersion of
15 local air pollutants.



16



1
 2 **Figure 3.** Model simulated 10 m wind vectors (arrows) and wind speed (shaded, unit: m s^{-1}), and
 3 the distribution of air mass concentrations (unit: $\text{mass hr}^{-1} \text{m}^{-3}$) within surface 100 m simulated
 4 by HYSPLIT Lagrangian backward particle release model with WS and TC as the starting points
 5 two days (20 Sept. 2013) before (a, c) and one day (21 Sept. 2013) before (b, d) the arrival of
 6 Usagi.

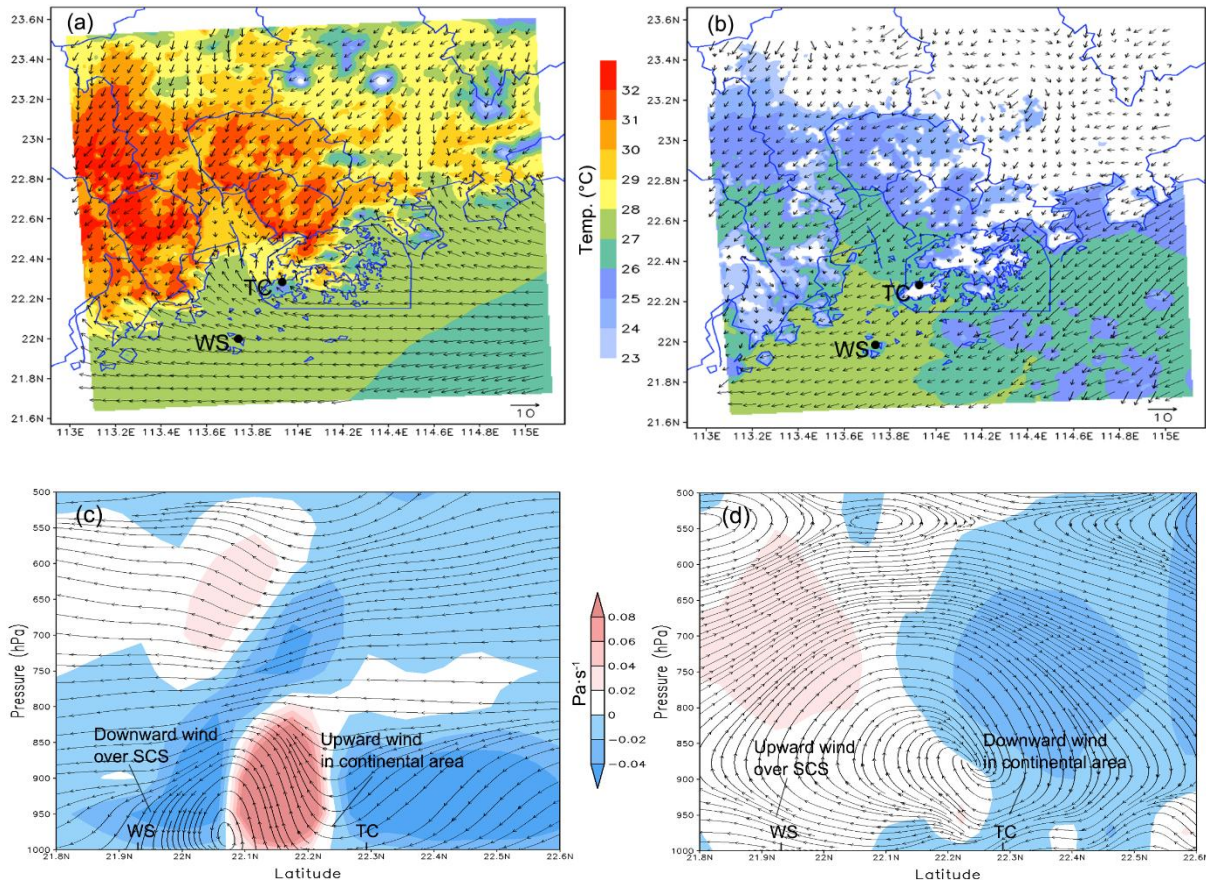
7
 8 *3.2.2 Continental anticyclones*

9 In addition to tropical cyclones, the continental anticyclone (high-pressure system) was
 10 frequently observed in the region, which often caused high O_3 concentrations. For example, two
 11 multi-day O_3 episodes (1-8 Oct. and 19-27 Oct.) occurred at the sampling sites when there were
 12 intensive continental anticyclones and weak Western Pacific Subtropical High (WPSH) to the
 13 north of Hong Kong (see Figure S5 as examples). The SLBs also occurred occasionally during
 14 the first several days of the two continental high pressure systems when the synoptic winds were
 15 relatively weak (*i.e.*, 2-5 Oct. and 19-21 Oct.). The clockwise and slow movement of the air
 16 masses caused northeasterly and easterly winds to the sampling sites and brought in densely
 17 polluted air from the inland (Figure 2b) to the coastal areas of the SCS. For example, the CO
 18 mixing ratios were significantly elevated during these episode days, with an average of 409 and
 19 683 ppbv at WS and TC, respectively, which were higher than other episode days. The
 20 continuous input of exotic air pollutants provided essential “fuel” to local photochemical
 21 production of O_3 , leading to the severe multi-day O_3 episodes.

1 3.2.3 Sea-land breeze (SLB) circulation

2 During the sampling period, SLB circulations in the study area were identified on 21 out of 104
3 sampling days. The occurrence frequency was comparable to that reported by Zhang and Zhang
4 (1997) who discovered 70 SLB days in a year in the same region. In this study, 12 O₃ episode
5 days were thought to be influenced by SLB (see Table S4), with 5 of them (27-28 Sept., 11-12
6 Oct. and 1 Nov.) under the dominance of tropical cyclones (*i.e.*, Wutip, Nari and Krosa) and the
7 other 7 days in association with the continental anticyclones. In addition to the effects of tropical
8 cyclones and continental anticyclones discussed above, SLB also posed non-negligible impact on
9 O₃ pollution in these cases.

10 SLB circulation is driven by sea-land thermal difference and topographic conditions, and usually
11 happens when the synoptic winds are weak (Liu et al., 2002; Lo et al., 2006; Lu et al., 2009b).
12 On a typical SLB day, wind blows onshore during the day (sea breeze) and offshore in the
13 evening (land breeze). However, the transition time of breezes in this study was found to vary in
14 a wide range. The sea breeze switched to land breeze between 00:00 and 08:00 with a median of
15 03:00 for breeze shifting, and 11:00 – 18:00 with the median of 14:00 was the time when land
16 breeze turned to sea breeze. Ding et al. (2004) also reported this phenomenon and pointed out
17 that the start time of sea breezes in Hong Kong was generally delayed to noontime due to the
18 synoptic northerly winds blowing from the continental areas to SCS, particularly on O₃ episode
19 days when northerly winds dominated in Hong Kong. For example, the sea breeze commenced at
20 15:00 on 3 Oct. and transited to land breeze at 4:00 on 4 Oct. (Figure 4). Figures 4a and 4b
21 depict the surface wind fields with a sea breeze and a land breeze, respectively. The vertical wind
22 fields with the sea breeze and land breeze are presented in Figures 4c and 4d, respectively.
23 Surface and vertical SLB circulations were clearly seen in these panels of Figure 4. The
24 mesoscale circulations caused by SLB might promote the interactions between the continental
25 (TC) and marine (WS) atmospheres. Specifically, the primary air pollutants observed at TC
26 could be transported to WS by land breeze. Moreover, the air masses could return to TC after
27 sufficient photochemical evolutions over SCS, during which O₃ might also be elevated in the
28 continental areas.



1
2
3 **Figure 4.** SLB circulation on 3-4 Oct. 2013, showing surface wind pattern (arrows) and
4 temperature (color) at 17:00 on 3 Oct. (a) and at 04:00 on 4 Oct. (b). Vertical cross-section
5 (taken over a longitude of 113.85°E, mean of the longitudes of TC and WS) depicting the v-w
6 wind stream (arrow) and the index of $\omega * 100$ (color) at 17:00 on 3 Oct. (c); and at 04:00 on 4
7 Oct. (d). For figures (c) and (d), the blue color (negative) and light red color (positive) present
8 downward and upward winds, respectively. Figures (a) and (c) represent a sea breeze, and
9 Figures (b) and (d) show a land breeze. Note that ω is the vertical velocity in isobaric
10 coordinates.

11 3.3 Chemical characteristics of air masses

12 3.3.1 Chemical composition

13 To inspect the chemical characteristics of air masses on O₃ episode days and non-O₃ episode
14 days, chemical species are statistically summarized at the two sites (Table 3). As expected, the
15

1 levels of all pollutants (*i.e.*, O₃, NO₂, CO, SO₂, NMHCs and carbonyls) were significantly higher
2 on O₃ episode days for both sites ($p < 0.05$), except for the comparable or even lower NO due to
3 its titration to O₃ (see Section 3.3.2). **Table S5 shows statistics of the top 10 NMHC and the top 3**
4 **carbonyl species observed during O₃ episodes and non-episodes at the two sites.** The dominant
5 species were quite similar regardless of episode or non-episode days at both sites. The higher
6 concentrations of both primary and secondary pollutants on episode days than those on non-
7 episode days were likely due to more intense photochemical reactions, more local pollutant
8 accumulation as well as the regional transport of more highly polluted air masses. On the other
9 hand, the similar NMHCs composition at both sites during both episodes and non-episodes
10 indicated somewhat interaction of air masses between the two sites regardless of O₃ levels.

11 It is worth to mention that O₃ was much higher at WS than that at TC during both episodes and
12 non-episodes ($p < 0.01$), with an average difference of 30.2 ppbv and 16.7 ppbv, respectively
13 (Table 3), though the levels of O₃ precursors (*i.e.*, NO_x and VOCs) at WS were lower. Insight
14 into VOC ratios found that ethene/ethane (0.5 ± 0.04) and toluene/benzene (2.2 ± 0.5) at WS were
15 significantly ($p < 0.05$) lower than those at TC (0.7 ± 0.1 and 2.9 ± 0.4 , respectively), likely
16 indicating that the air masses at WS were more aged (Guo et al., 2007). Therefore, the higher O₃
17 at WS might be partially attributable to the aging of air masses (*e.g.*, during the transport of
18 continental air).

1 **Table 3.** Descriptive statistics (Mean \pm 95% *C.I.*) of measured air pollutants, simulated OH,
 2 **HO₂ and RO₂** at the two sites during O₃ episodes and non-O₃ episodes days.

Parameter	WS		TC	
	<i>O₃ episode</i>	<i>Non-O₃ episode</i>	<i>O₃ episode</i>	<i>Non-O₃ episode</i>
O ₃ (ppbv)	74.3 \pm 3.0	43.9 \pm 1.0	44.1 \pm 3.6	27.2 \pm 0.8
O _x (ppbv)	81.6 \pm 2.9	47.8 \pm 1.0	83.3 \pm 3.7	49.4 \pm 1.0
NO (ppbv)	0.9 \pm 0.2	0.5 \pm 0.2	11.5 \pm 1.4	14.5 \pm 0.9
NO ₂ (ppbv)	8.5 \pm 0.9	2.0 \pm 0.5	39.2 \pm 1.7	22.2 \pm 0.6
CO (ppbv)	391.4 \pm 9.1	209.4 \pm 6.8	652.9 \pm 16.0	541.9 \pm 6.5
SO ₂ (ppbv)	4.3 \pm 0.2	1.9 \pm 0.1	8.1 \pm 0.3	5.5 \pm 0.1
NMHCs (ppbv)	17.7 \pm 1.4	9.6 \pm 1.2	20.2 \pm 2.2	16.8 \pm 2.1
Carbonyls (ppbv)	10.3 \pm 0.8	5.4 \pm 0.4	12.0 \pm 1.3	8.1 \pm 0.7
NO ₂ /NO (ppbv/ppbv)	12.7 \pm 1.1	4.7 \pm 0.5	3.4 \pm 0.4	1.5 \pm 0.2
Simulated OH ($\times 10^6$ molecules cm ⁻³)	5.5 \pm 0.9	4.4 \pm 0.6	1.5 \pm 0.4	2.1 \pm 0.3
Simulated HO ₂ ($\times 10^7$ molecules cm ⁻³)	29 \pm 4.9	45 \pm 4.2	2.0 \pm 1.0	2.6 \pm 0.7
Simulated RO ₂ ($\times 10^7$ molecules cm ⁻³)	19 \pm 3.8	47 \pm 6.2	1.2 \pm 0.6	1.4 \pm 0.4

3 * Average of the daily maximum solar radiation. *C.I.* denotes confidence interval. O_x = O₃ + NO₂.

5 3.3.2 Influence of NO titration

6 Apart from the age of air masses, NO titration is another important factor influencing O₃
 7 concentration. In areas with high NO levels, the NO titration (O₃ + NO \rightarrow NO₂ + O₂) is a
 8 main process consuming O₃. In this study, the average NO mixing ratio at TC was 14.0 \pm 0.8
 9 ppbv, compared to 0.7 \pm 0.1 ppbv at WS (Table 1). **The much lower NO at WS implied**
 10 **weaker titration to O₃, which enabled the survival of more O₃ and caused substantial residual**
 11 **O₃ at WS particularly at night time when there were no photochemical reactions (Figure 2**
 12 **and Figure S6).** Another direct evidence of NO titration effect was the trough of O₃ during
 13 the morning rush hours (06:00-07:00), together with an increase of NO₂ (Figure S6).

1 Furthermore, the total oxidants ($O_x = O_3 + NO_2$), which are usually adopted to take into
2 account the NO titration influence, were comparable ($p > 0.05$) between TC and WS with
3 mean values of 83.3 ± 3.7 ppbv and 81.6 ± 2.9 ppbv during O_3 episodes, and 49.4 ± 1.0 ppbv and
4 47.8 ± 1.0 ppbv during non-episodes, respectively (Table 3). This was reasonable in view of
5 the interactions between the two sites. However, the remarkably higher O_3 and lower NO at
6 WS indicated that NO titration was a determinant factor regulating the O_3 levels at both sites.

7 Moreover, NO titration is generally more significant on high O_3 days, resulting in higher
8 NO_2/NO ratios due to the conversion of NO to NO_2 by O_3 . Indeed, the mean NO_2/NO ratios
9 increased from 4.7 ± 0.5 at WS and 1.5 ± 0.2 at TC during non-episodes to 12.7 ± 1.1 and
10 3.4 ± 0.4 during O_3 episodes, respectively, implying that more O_3 was titrated by NO during
11 episodes. As a result, NO at TC was lower ($p < 0.01$) during O_3 episodes than during non-
12 episodes (Table 3). It is noteworthy that NO at WS was on the same level between O_3 episode
13 and non- O_3 episode days ($p > 0.05$). This probably related to the weak titration at this marine
14 site due to the trivial NO concentrations in both periods, as well as the counteracting effect of
15 the increased transport of NO under northerly winds against the enhanced titration during O_3
16 episodes.

17 The aforementioned discussion demonstrated that NO titration played an important role in
18 altering O_3 distribution, especially on O_3 episodes days. The lower NO (weaker NO titration)
19 partially resulted in the higher O_3 concentrations observed at WS.

20 *3.3.3 Atmospheric oxidative capacity and O_3 production rate*

21 O_3 formation is driven by the transformation and recycling of oxidative radicals, including
22 OH, HO_2 and RO_2 , collectively referred to as RO_x hereafter. The production and loss rates of
23 these radicals, and their equilibrium concentrations on the canister sampling days were
24 simulated by the PBM-MCM model, as shown in Figure S7. We noticed that WS featured
25 significantly higher levels of these oxidative radicals on average ($p < 0.05$). The daytime
26 (7:00-19:00 LT) average OH concentration at TC and WS was $(1.5 \pm 0.4) \times 10^6$ molecules cm^{-3}
27 and $(5.5 \pm 0.9) \times 10^6$ molecules cm^{-3} during O_3 episodes, respectively. Consistently, HO_2 and
28 RO_2 at WS were well above those at TC (Table 3). This pattern was also applicable between
29 the two sites during non-episodes. Furthermore, while the difference in OH concentration
30 became less on non-episode days, the gaps for peroxy radicals (HO_2 and RO_2) between TC
31 and WS widened, as listed in Table 3. From non-episodes to episodes, OH increased at WS
32 alongside with the decreases of HO_2 and RO_2 , likely indicating more conversion of HO_2 to

1 | OH by NO₂ which is an important pathway leading to O₃ formation. Details about this were
2 | shown later.

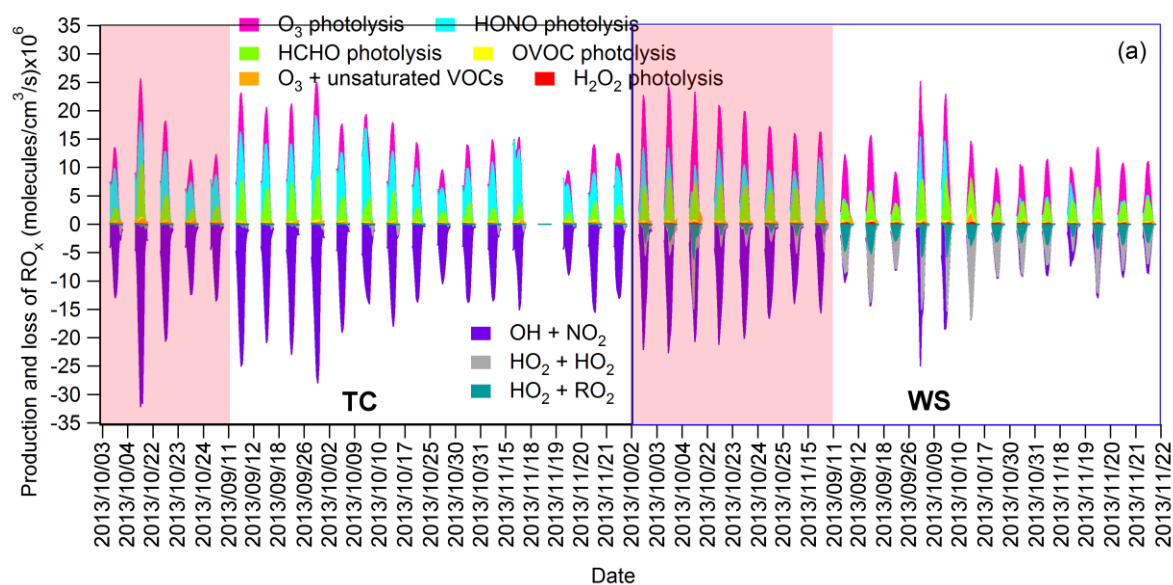
3 | To explain the inter-site differences of the concentrations of oxidative radicals and the
4 | variations between O₃ episodes and non-episodes, [Figure S7](#) also provides the breakdowns of
5 | the production and loss rates of OH, HO₂ and RO₂ at TC and WS, separately. Overall, the
6 | reaction between HO₂ and NO dominated the production of OH at both sites, with the
7 | contribution of 69.4±2.0% and 81.0±1.5% at TC and WS, respectively. While the photolysis
8 | of HONO ranked the second in the production of OH at TC (22.2±2.1%), the contribution of
9 | this pathway to OH production at WS (3.7±0.6%) was overstepped by O₃ photolysis
10 | (13.1±1.6%). This discrepancy was associated with the higher HONO and lower O₃ at TC
11 | ([Figure S1](#) and [Table 3](#)). As expected, the production rate of OH through HO₂ reacting with
12 | NO experienced the most significant increase from 1.4±0.2×10⁷ molecules cm⁻³ s⁻¹ during
13 | non-episodes to 3.6±0.6×10⁷ molecules cm⁻³ s⁻¹ during O₃ episodes at WS, which explained
14 | more than 90% of the increase of the total OH production. In terms of the losses of OH,
15 | reaction between OH and NO₂ was the largest sink of OH at TC. However, OH-initiated
16 | oxidations of VOCs consumed most (52.7±1.8%) of OH at WS. This was reasonable in view
17 | of the much more abundant NO₂ at TC than at WS, in contrast to the smaller difference in
18 | NMHCs between the two sites ([Table 3](#)). Since OH can generally be recycled from the
19 | oxidation of VOCs, the lower OH at TC was likely caused by the lower O₃ photolysis and
20 | higher consumption of OH by NO₂, despite the more intensive HONO photolysis. The overall
21 | oxidation rate of VOCs by OH was employed to indicate the atmospheric oxidative capacity
22 | in previous studies (Elshorbany et al., 2009; Xue et al., 2016). In this study, we found that the
23 | oxidation rate of VOCs at TC (6.1±2.1×10⁶ molecules cm⁻³ s⁻¹ during O₃ episodes and
24 | 5.7±0.9×10⁶ molecules cm⁻³ s⁻¹ during non-episodes) was remarkably (*p*<0.05) lower than
25 | that at WS (O₃ episode: 15±2.5×10⁶ molecules cm⁻³ s⁻¹ and non-episode: 8.9±1.3×10⁶
26 | molecules cm⁻³ s⁻¹). The results revealed that the atmospheric oxidative capacity at TC was
27 | weaker than at WS for both O₃ episodes and non-episodes, inconsistent with the findings of
28 | Elshorbany et al. (2009) and Xue et al. (2016) who concluded that the atmospheric oxidative
29 | capacity was higher in more polluted environments due to the fact that the atmospheric
30 | oxidative capacity is positively proportional to the VOCs and OH levels. Both Elshorbany et
31 | al. (2009) and Xue et al. (2016) reported very high mixing ratios of VOCs (*e.g.* toluene of 9.5
32 | and 6.3 ppbv, respectively) in the polluted cases, which explained the strong atmospheric
33 | oxidative capacity. However, in this study, it is more likely that the higher NO_x at TC

1 consumed more OH and resulted in lower oxidative capacity than at WS, despite the slightly
2 higher VOCs at TC (Table 3).

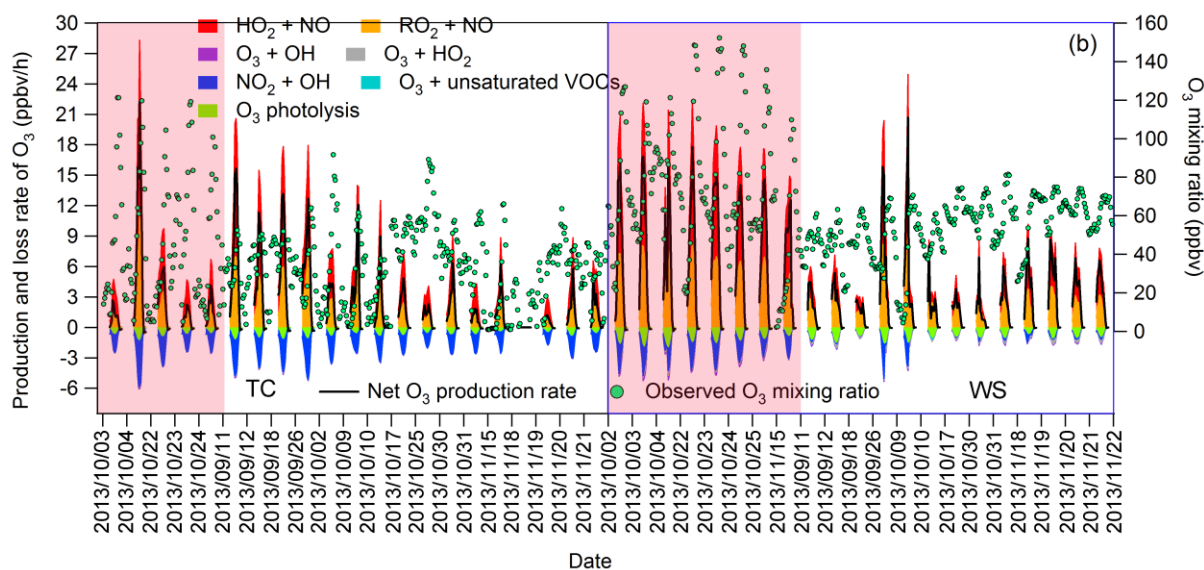
3 For HO₂, RO₂ reacting with NO accounted for 56.7±1.1% and 60.7±1.0% of HO₂ production
4 at TC and WS, respectively. Oxidation of CO by OH was also an important pathway leading
5 to HO₂ formation, second to RO₂+NO at both sites. At TC, HO₂ was almost exclusively
6 depleted by NO. However, 10.8±1.8% and 6.5±0.8% of the HO₂ losses were attributable to
7 HO₂-RO₂ and HO₂-HO₂ reactions at WS, respectively, though HO₂+NO was responsible for
8 the most fraction (82.7±2.6%) of HO₂ losses. We believe that the more significant self-
9 consumption of peroxy radicals at WS was closely related to the low NO_x there, which
10 hampered the transfer of oxygen atom from peroxy radicals to NO and further formation of
11 O₃. This was confirmed by the enhanced losses of HO₂ through reactions with HO₂ itself and
12 RO₂ from 3.0±1.2% during O₃ episodes to 24.9±3.4% during non-episodes at WS, because
13 NO_x was more scarce during non-episodes at this site (Table 3). Similarly, in contrast to the
14 negligible influence of RO₂ reacting with HO₂ on RO₂ budget at TC, HO₂-RO₂ reactions
15 played important role in losses of RO₂ at WS, particularly on non-episode days (Figure S7).
16 When OH, HO₂ and RO₂ were summed up, the production and loss rate of RO_x were obtained,
17 as shown in Figure 5(a). Under such circumstance, the transformation and recycling pathways
18 among these radicals can be neglected. For example, OH-initiated oxidation of VOCs
19 consumes OH, which however generates RO₂. Therefore, these reactions were not considered
20 as sources or sinks of RO_x. On one hand, HONO photolysis was the largest source of RO_x at
21 TC (53.7±2.6%), followed by the photolysis of HCHO (21.1±1.6%) and O₃ (18.7±1.5%).
22 However, O₃ photolysis ranked the first among the sources of RO_x at WS with the
23 contribution of 38.6±2.3%, higher than the contributions from HCHO photolysis (34.3±1.4%)
24 and HONO photolysis (18±2.5%). On the other hand, while the reaction between OH and
25 NO₂ served as the sole sink of RO_x at TC, it only explained 50% of RO_x sink at WS with the
26 other half attributable to self-consumption of peroxy radicals.

27 Furthermore, the production and loss rates of O₃ were simulated (Figure 5(b)). Despite the
28 increased O₃ mixing ratio during episodes (Table 3), there was no significant change in net
29 O₃ production between O₃ episodes (2.5±1.0 ppbv/h) and non-episodes (2.5±0.5 ppbv/h) at
30 TC ($p>0.05$), suggesting that regional transport might play critical roles in regulating O₃
31 levels at TC. In fact, previous studies (Huang et al., 2006; Jiang et al., 2008) have repeatedly
32 confirmed that O₃ pollution at this site could be aggravated under northerly winds and/or

1 downdraft on the periphery of typhoon. In contrast, the net O₃ production increased
 2 remarkably from non-episodes (2.8 ± 0.5 ppbv/h) to O₃ episodes (6.6 ± 1.1 ppbv/h) at WS.
 3 Obviously, O₃ production at WS was much higher than at TC during O₃ episodes, while they
 4 were comparable during non-episodes. This was likely due to the more abundant peroxy
 5 radicals (RO₂ and HO₂) at WS than at TC, in addition to the increased NO_x during O₃
 6 episodes which enhanced the reactions between the peroxy radicals and NO (increasing O₃
 7 formation). Insight into the O₃ production pathways found that the reaction rates of RO₂+NO
 8 and HO₂+NO were significantly enhanced from 1.6 ± 0.2 and 2.0 ± 0.4 ppbv/h during non-
 9 episodes to 3.2 ± 0.5 and 5.2 ± 0.9 ppbv/h during O₃ episodes, respectively. Our recent study
 10 (Wang et al., 2017b) revealed that O₃ formation at WS was in a transition regime and much
 11 more sensitive to NO_x during non-episodes, when O₃ production through peroxy radicals
 12 reacting with NO was seriously limited by the low NO_x. During O₃ episodes, with the
 13 increase O₃ precursors (particularly NO_x), these reactions were accelerated and the net O₃
 14 production increased substantially. Detailed discussion on the O₃ photochemistry at WS can
 15 be found in our recent publication (Wang et al., 2017b).



16

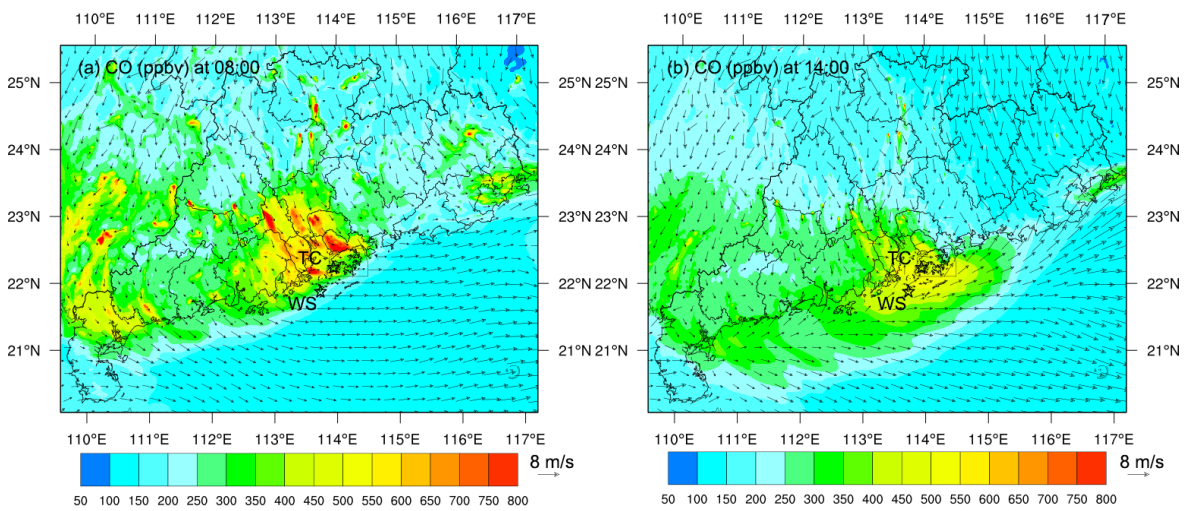


1
 2 **Figure 5.** Daytime (7:00-19:00 LT) variations of the simulated production and loss rates of (a)
 3 RO_x and (b) O_3 at TC (left panel) and WS (right panel). O_3 episode days are highlighted in
 4 red background. The dates are not consecutive due to the discontinuous canister sampling of
 5 $VOCs$.

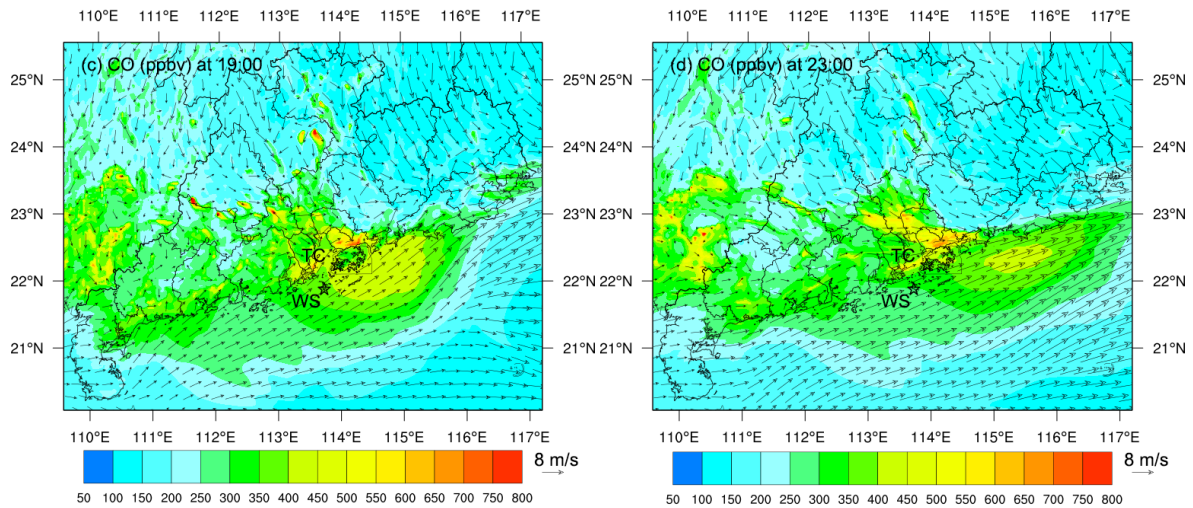
6 3.4 Impact of air mass interaction on O_3 pollution in coastal areas

7 Driven by various weather systems (*e.g.*, continental anticyclones, WPSH, tropical cyclones
 8 and SLBs), continental and marine air masses frequently interact with each other in the
 9 coastal areas. When continental air masses intrude into marine atmosphere, the chemical
 10 composition and atmospheric oxidative capacity over the marine atmosphere will be altered
 11 by the introduction of anthropogenic pollutants. Taken 21 Aug. as an example, when the
 12 sampling sites (TC and WS) were under northwesterly to southwesterly winds caused by
 13 tropical cyclone (Figure 2a), the maximum hourly O_3 reached 160 and 173 ppbv at TC and
 14 WS, respectively. Correspondingly, the primary air pollutants all stayed on high levels,
 15 compared to those during non-episodes (Figure 2a). Since WS was almost free of
 16 anthropogenic emissions, the great abundances of both primary and secondary air pollutants
 17 implied the influence of continental pollution on air quality at this site. Figures 6-7 depict the
 18 spatial distributions of CO and O_3 over the region of interest at selective time (08:00, 14:00,
 19 19:00 and 23:00) on 21 Aug., respectively. CO is presented as an example of primary air
 20 pollutants emitted from anthropogenic sources. The spatiotemporal patterns of CO and O_3
 21 were simulated by WRF-CMAQ. Noticeably, the model well reproduced high level of CO in
 22 PRD region at 08:00, which was reasonable in view of the vehicular emissions in urban areas

1 during morning rush hours. However, under the dominance of northwesterly winds in the
 2 morning, the center of high CO moved to the coastal areas. Even though the winds changed
 3 to southwesterly at noon, CO concentration over SCS was still remarkably elevated according
 4 to the simulated results at 14:00. Further, the spatial distribution of CO at 19:00 and 23:00
 5 confirmed the continuous movement of the polluted air masses away from the land under
 6 southwesterly winds. It should be noted that the increase of CO in PRD region at 19:00 and
 7 23:00 were most likely caused by the vehicle emissions during evening rush hours. Overall,
 8 the dynamic distribution of CO in the study area clearly indicated the interaction between
 9 continental and marine atmospheres. As a result of the intrusion of continental air, high level
 10 of O₃ was simulated over SCS at 14:00 (Figure 7b), which was comparable to the observed
 11 value (148 ppbv) at WS. Moreover, O₃ was even higher over SCS than that in continental
 12 area, due mainly to the more aged air masses, lower NO titration and higher oxidative
 13 capacity of the atmosphere (see section 3.3). Consistent with CO, the center of high O₃
 14 moved away from the land. At 19:00, the O₃-laden air mass penetrated into the SCS ~300 km,
 15 causing ~8,000 km² water area (8 times the area of Hong Kong) under high level of O₃ (>100
 16 ppbv). This case provided solid evidence of the transport of continental air masses to SCS,
 17 which aggravated air pollution (particularly O₃ pollution) in this offshore area.

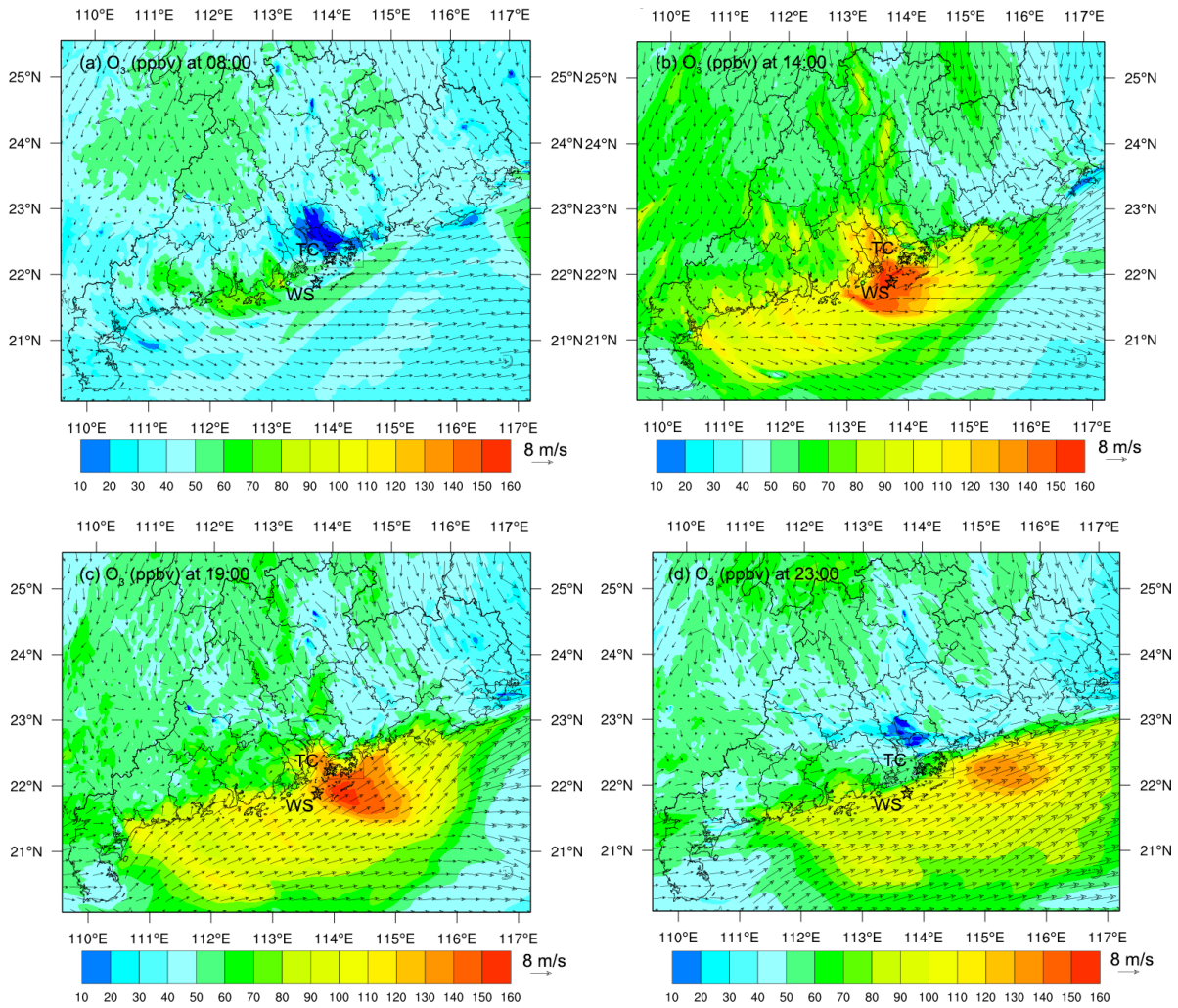


18



1

2 **Figure 6.** Spatial distribution of CO at 08:00 (a), 14:00 (b), 19:00 (c) and 23:00 (d) on 21
 3 August simulated by WRF-CMAQ, taken as an example of the “Outflow” interaction pattern.
 4 Arrows in the figure represent the surface wind field.



5

6 **Figure 7** Spatial distribution of O₃ at 08:00 (a), 14:00 (b), 19:00 (c) and 23:00 (d) on 21
 7 August simulated by WRF-CMAQ, taken as an example of the “Outflow” interaction pattern.
 8 Arrows in the figure represent the surface wind field.
 9

1 In contrast to outflow of continental air masses, the continental area near the coast could also
2 be immersed by oceanic air masses. The arrival of oceanic air masses generally brings
3 substantial marine-originated compounds (e.g. dimethyl sulfide) to the continent and
4 significantly alleviates the anthropogenic air pollution there. In fact, this is one of the main
5 reasons for low O₃ mixing ratio observed in the PRD region in summertime when
6 southwestern winds prevail (Wang et al., 2009; Wang et al., 2017a). In this study, it was also
7 found that winds over the ocean increased the concentration of dimethyl sulfide at TC (Figure
8 S8) and reduced the levels of almost all man-made air pollutants in many cases, mainly in
9 summertime (Figure 2a).

10 In contrast, sea breezes carrying elevated O₃ formed over SCS might build up the terrestrial
11 O₃ in the coastal area in some cases. Figure 8 shows the spatial distribution of O₃ over the
12 study area on 3 Oct., as an example of SLB regulating O₃ formation and distribution (see
13 Figure 4). Similar to the aforementioned scenario controlled by tropical cyclone, the
14 simulated O₃ at 14:00 was generally higher over SCS than in the terrestrial area, indicating
15 the transport of polluted air masses from the land to the sea area. This was confirmed by the
16 prevailing northeasterly winds in the morning (08:00 here). However, the O₃-laden air did not
17 move far away from the land subsequently. Instead, it progressively approached the land,
18 leading to increase of O₃ concentration in most parts of Hong Kong. This is because the wind
19 direction in the coastal region changed from northeasterly to southeasterly at 17:00. Namely,
20 the sea breeze appeared in late afternoon, which delivered the high O₃ formed over SCS to
21 the continental areas near the coast. In fact, the air quality monitoring stations deployed in
22 southern Hong Kong by HKEPD also recorded the O₃ peak in the evening when O₃ could not
23 be formed locally (Figure S9), further confirming the recirculation of O₃-laden air from SCS
24 to coastal areas of Hong Kong under sea-breeze. However, the oceanic air did not penetrate
25 further into the inland PRD, which was likely stopped by the strong northeasterly winds
26 dominated in the inland areas. Overall, it can be seen that SLB as a common interaction
27 between marine and continental atmospheres played important role in regulating O₃
28 formation and distribution in coastal region of SCS, which is also applicable to other similar
29 mesoscale environments over the world.

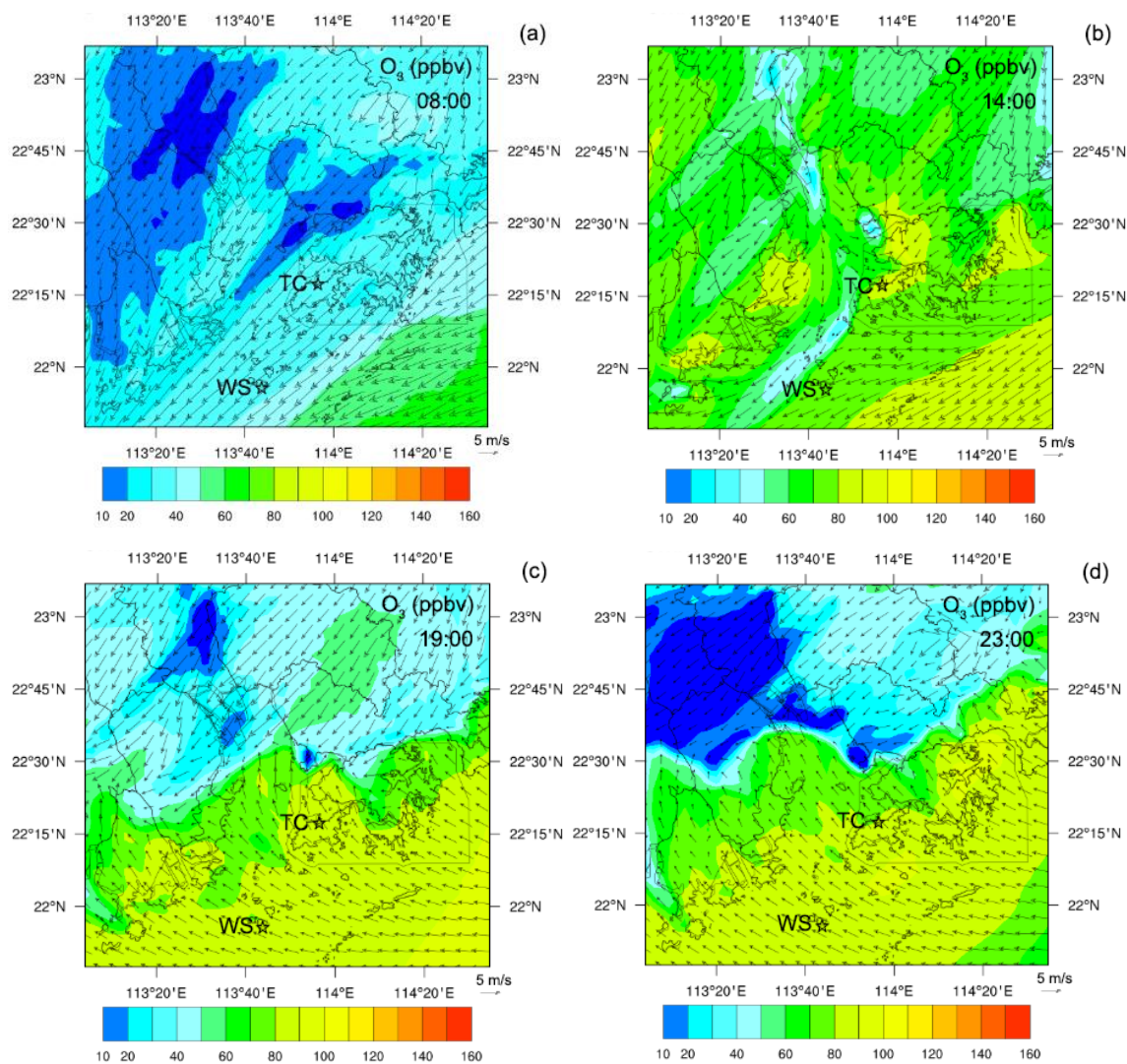


Figure 8. Spatial distribution of O_3 at 08:00 (a), 14:00 (b), 19:00 (c) and 23:00 (d) on 3 October, taken as an example of the “SLB” interaction pattern. Arrows in the figure represent the surface wind field.

4. Conclusions

Coastal regions with dense population, economic prosperity and environmental pollution are common in the world. This study provided an overview of O_3 pollution in warm seasons around a coastal region of SCS, focusing on the influences of interactions between marine and continental atmospheres on air quality in this subtropical region. The concurrent measurements of primary and secondary air pollutants at TC (a continental site) and WS (a marine site) from August to November 2013 indicated that O_3 was much higher at WS than that at TC, contrary to the more abundant primary air pollutants at TC. At the two sites, O_3 episodes and near- O_3 episodes were frequently observed, which were closely associated with

1 continental anticyclone, tropical cyclone and SLB. In addition to high temperature, strong
2 solar radiation and weak wind, the aforementioned meteorological conditions all favored the
3 transport of polluted air masses from continental areas to SCS, during which the air pollutants
4 were transformed with the aging of air masses. After arriving in SCS, the land-originated air
5 pollutants further involved in intensive photochemical reactions with the trait of low NO
6 titration to O₃ and high O₃ production rate, leading to higher O₃ level in marine atmosphere
7 (WS) than that in coastal cities (TC). In addition to the continental outflow that aggravated O₃
8 pollution over SCS, SLB as a common interaction in coastal areas also often facilitated the
9 recirculation of O₃ formed over SCS to the continental areas, building up O₃ concentration in
10 coastal cities under sea breeze. The findings can be extended to other similar regions to
11 advance our understanding of O₃ pollution.

12 **Acknowledgements**

13 This project was supported by the Natural Science Foundation of China (Grant No.
14 41275122), the Research Grants Council (RGC) of the Hong Kong Government of Special
15 Administrative Region (PolyU5154/13E, PolyU152052/14E, PolyU152052/16E and
16 CRF/C5004-15E), the Guangdong special fund for science and technology development
17 (2017B020216007), and partly by the Hong Kong PolyU internal grant (G-SB63, 1-BBW4
18 and 4-ZZFW). The authors thank HKEPD for provision of the air quality and meteorological
19 data at TC site, and are grateful to Po On Commercial Association Wan Ho Kan Primary
20 School at Tung Chung and the National Marine Environmental Monitoring Station at
21 Wanshan Island for their generous support on the field study. Contributions to field
22 measurements by Kalam Cheung, Dawei Wang, Bo Liu, Nan Wang, Jiamin Ou, Huanghuang
23 Yan and Xiaoxin Fu are also highly appreciated. The authors also gratefully acknowledge the
24 NOAA Air Resources Laboratory (ARL) for the provision of the HYSPLIT transport and
25 dispersion model and/or READY website (<http://www.ready.noaa.gov>), and Prof. Tao
26 Wang's group of The Hong Kong Polytechnic University for the provision of the average
27 diurnal profiles of HONO at TC and HT.

28 **References**

29 Adame, J. A., Serrano, E., Bolívar, J. P., and de la Morena, B. A.: On the Tropospheric
30 Ozone Variations in a Coastal Area of Southwestern Europe under a Mesoscale Circulation,

1 Journal of Applied Meteorology and Climatology, 49, 748-759, 10.1175/2009jamc2097.1,
2 2010.

3 Bell, M. L., Goldberg, R., Hogrefe, C., Kinney, P. L., Knowlton, K., Lynn, B., Rosenthal, J.,
4 Rosenzweig, C., and Patz, J. A.: Climate change, ambient ozone, and health in 50 US cities,
5 Climatic Change, 82(1-2), 61-76, 2007.

6 Cabaraban, M. T. I., Kroll, C. N., Hirabayashi, S., and Nowak, D. J.: Modeling of air
7 pollutant removal by dry deposition to urban trees using a WRF/CMAQ/i-Tree Eco coupled
8 system, Environmental pollution, 176, 123-133, 2013.

9 | Chan, C. Y.: Effects of Asian air pollution transport and photochemistry on carbon monoxide
10 variability and ozone production in subtropical coastal south China, Journal of Geophysical
11 Research, 107, 10.1029/2002jd002131, 2002.

12 | Cheng, H., Guo, H., Saunders, S., Lam, S., Jiang, F., Wang, X., Simpson, I., Blake, D., Louie,
13 P., and Wang, T.: Assessing photochemical ozone formation in the Pearl River Delta with a
14 photochemical trajectory model, Atmospheric Environment, 44, 4199-4208, 2010b.

15 | Cheng, H., Guo, H., Wang, X., Saunders, S. M., Lam, S. H. M., Jiang, F., Wang, T., Ding, A.,
16 Lee, S., and Ho, K.: On the relationship between ozone and its precursors in the Pearl River
17 Delta: application of an observation-based model (OBM), Environmental Science and
18 Pollution Research, 17, 547-560, 2010a.

19 | Cui, J., Deolal, S. P., Sprenger, M., Henne, S., Staehelin, J., Steinbacher, M., and Nedelec, P.:
20 Free tropospheric ozone changes over Europe as observed at Jungfraujoch (1990-2008): An
21 analysis based on backward trajectories, Journal of Geophysical Research - Atmospheres,
22 116, 2011.

23 | Derwent, R. G., Manning, A. J., Simmonds, P. G., Spain, T. G., and O'Doherty, S.: Analysis
24 and interpretation of 25 years of ozone observations at the Mace Head Atmospheric Research
25 Station on the Atlantic Ocean coast of Ireland from 1987 to 2012, Atmospheric Environment,
26 80, 361-368, 10.1016/j.atmosenv.2013.08.003, 2013.

27 | Ding, A. J., Wang, T., Zhao, M., Wang, T. J., and Li, Z. K.: Simulation of sea-land breezes
28 and a discussion of their implications on the transport of air pollution during a multi-day
29 ozone episode in the Pearl River Delta of China, Atmospheric Environment, 38, 6737-6750,
30 10.1016/j.atmosenv.2004.09.017, 2004.

1 | Ding, A. J., Wang, T., Thouret, V., Cammas, J. P., and Nedelec, P.: Tropospheric ozone
2 | climatology over Beijing: analysis of aircraft data from the MOZAIC program, *Atmospheric*
3 | *Chemistry and Physics*, 8, 1-13, 2008.

4 | Ding, A. J., Fu, C. B., Yang, X. Q., Sun, J. N., Zheng, L. F., Xie, Y. N., Herrmann, E., Nie,
5 | W., Petäjä T., Kerminen, V. M., and Kulmala, M.: Ozone and fine particle in the western
6 | Yangtze River Delta: An overview of 1 yr data at the SORPES station, *Atmospheric*
7 | *Chemistry and Physics*, 13, 5813-5830, 10.5194/acp-13-5813-2013, 2013b.

8 | Ding, A. J., Wang, T., and Fu, C. B.: Transport characteristics and origins of carbon
9 | monoxide and ozone in Hong Kong, South China, *Journal of Geophysical Research -*
10 | *Atmospheres*, 118, 9475-9488, 2013a.

11 | Draxler, R. R., and Rolph, G. D.: HYSPLIT (HYbrid Single-Particle Lagrangian Integrated
12 | Trajectory) Model access via NOAA ARL READY Website
13 | (<http://www.arl.noaa.gov/ready/hysplit4.html>). , NOAA Air Resources Laboratory, Silver
14 | Spring, Maryland, USA, 2003.

15 | Dunlea, E. J., Herndon, S. C., Nelson, D. D., Volkamer, R. M., San Martini, F., Sheehy, P.
16 | M., Zahniser, M. S., Shorter, J. H., Wormhoudt, J. C., Lamb, B. K., Allwine, E. J., Gaffney, J.
17 | S., Marley, N. A., Grutter, M., Marquez, C., Blanco, S., Cardenas, B., Retama, A., Villegas,
18 | C. R. R., Kolb, C. E., Molina, L. T., and Molina, M. J.: Evaluation of nitrogen dioxide
19 | chemiluminescence monitors in a polluted urban environment, *Atmospheric Chemistry and*
20 | *Physics*, 7, 2691-2704, DOI 10.5194/acp-7-2691-2007, 2007.

21 | Elshorbany, Y. F., Kurtenbach, R., Wiesen, P., Lissi, E., Rubio, M., Villena, G., Gramsch, E.,
22 | Rickard, A. R., Pilling, M. J., and Kleffmann, J.: Oxidation capacity of the city air of
23 | Santiago, Chile, *Atmospheric Chemistry and Physics*, 9(6), 2257-2273, 2009.

24 | Fowler, D., Pilegaard, K., Sutton, M. A., Ambus, P., Raivonen, M., Duyzer, J., Simpson, D.,
25 | Fagerli, H., Fuzzi, S., Schjoerring, J. K., Granier, C., Nefstel, A., Isaksen, I. S. A., Laj, P.,
26 | Maione, M., Monks, P. S., Burkhardt, J., Daemmgen, U., Neiryneck, J., Personne, E.,
27 | Wichink-Kruit, R., Butterbach-Bahl, K., Flechard, C., Tuovinen, J. P., Coyle, M., Gerosa, G.,
28 | Loubet, B., Altimir, N., Gruenhage, L., Ammann, C., Cieslik, S., Paoletti, E., Mikkelsen, T.
29 | N., Ro-Poulsen, H., Cellier, P., Cape, J. N., Horvath, L., Loreto, F., Niinemets, U., Palmer, P.
30 | I., Rinne, J., Misztal, P., Nemitz, E., Nilsson, D., Pryor, S., Gallagher, M. W., Vesala, T.,
31 | Skiba, U., Brüeggemann, N., Zechmeister-Boltenstern, S., Williams, J., O'Dowd, C., Facchini,

1 M. C., de Leeuw, G., Flossman, A., Chaumerliac, N., and Erisman, J. W.: Atmospheric
2 composition change: Ecosystems-Atmosphere interactions, *Atmospheric Environment*, 43,
3 5193-5267, 10.1016/j.atmosenv.2009.07.068, 2009.

4 Guenther, C. C.: Estimates of global terrestrial isoprene emissions using MEGAN (Model of
5 Emissions of Gases and Aerosols from Nature), *Atmospheric Chemistry and Physics*, 6,
6 3181-3210, 2006.

7 Guo, H., Jiang, F., Cheng, H. R., Simpson, I. J., Wang, X. M., Ding, A. J., Wang, T. J.,
8 Saunders, S. M., Wang, T., Lam, S. H. M., Blake, D. R., Zhang, Y. L., and Xie, M.:
9 Concurrent observations of air pollutants at two sites in the Pearl River Delta and the
10 implication of regional transport, *Atmospheric Chemistry and Physics*, 9, 7343-7360, 2009.

11 Guo, H., Ling, Z. H., Cheung, K., Jiang, F., Wang, D. W., Simpson, I. J., Barletta, B.,
12 Meinardi, S., Wang, T. J., Wang, X. M., Saunders, S. M., and Blake, D. R.: Characterization
13 of photochemical pollution at different elevations in mountainous areas in Hong Kong,
14 *Atmospheric Chemistry and Physics*, 13, 3881-3898, 10.5194/acp-13-3881-2013, 2013.

15 Guo, H., So, K. L., Simpson, I. J., Barletta, B., Meinardi, S., and Blake, D. R.: C₁-C₈ volatile
16 organic compounds in the atmosphere of Hong Kong: Overview of atmospheric processing
17 and source apportionment, *Atmospheric Environment*, 41(7), 1456-1472, 2007.

18 HKEPD: Air Quality in Hong Kong 2014, available at:
19 http://www.aqhi.gov.hk/api_history/english/report/files/AQR2014e_Update0616.pdf, Hong
20 Kong Environmental Protection Department, 2015.

21 Huang, J. P., Fung, J. C. H., Lau, A. K. H., and Qin, Y.: Numerical simulation and process
22 analysis of typhoon-related ozone episodes in Hong Kong, *Journal of Geophysical Research*,
23 110, 10.1029/2004jd004914, 2005.

24 Huang, J. P., Fung, J. C., and Lau, A. K.: Integrated processes analysis and systematic
25 meteorological classification of ozone episodes in Hong Kong, *Journal of Geophysical
26 Research - Atmospheres*, 111(D20), 2006.

27 IPCC: Climate Change 2014: Synthesis Report. Contribution of Working Groups I, II and III
28 to the Fifth Assessment Report of the Intergovernmental Panel on Climate Change, [Core
29 Writing Team, R.K. Pachauri and L.A. Meyer (eds.)], IPCC, Geneva, Switzerland, 151, 2014.

- 1 | Jenkin, M. E., Saunders, S. M., and Pilling, M. J.: The tropospheric degradation of volatile
2 | organic compounds: A protocol for mechanism development, *Atmospheric Environment*, 31,
3 | 81-104, 1997.
- 4 | Jenkin, M. E., Saunders, S. M., Wagner, V., and Pilling, M. J.: Protocol for the development
5 | of the Master Chemical Mechanism, MCM v3 (Part B): tropospheric degradation of aromatic
6 | volatile organic compounds, *Atmospheric Chemistry and Physics*, 3, 181-193, 2003.
- 7 | Jiang, F., Guo, H., Wang, T., Cheng, H., Wang, X., Simpson, I., Ding, A., Saunders, S., Lam,
8 | S., and Blake, D.: An ozone episode in the Pearl River Delta: Field observation and model
9 | simulation, *Journal of Geophysical Research*, 115, D22305, doi:10.1029/2009JD013583,
10 | 2010.
- 11 | **Jiang, F., Wang, T., Wang, T., Xie, M., and Zhao, H.: Numerical modeling of a continuous
12 | photochemical pollution episode in Hong Kong using WRF-chem, *Atmospheric
13 | Environment*, 42(38), 8717-8727, 2008.**
- 14 | Jiang, Y. C., Zhao, T. L., Liu, J., Xu, X. D., Tan, C. H., Cheng, X. H., Bi, X. Y., Gan, J. B.,
15 | You, J. F., and Zhao, S. Z.: Why does surface ozone peak before a typhoon landing in
16 | southeast China? *Atmospheric Chemistry and Physics*, 15, 13331-13338, 10.5194/acp-15-
17 | 13331-2015, 2015.
- 18 | He K.: Multi-resolution Emission Inventory for China (MEIC): model framework and 1990-
19 | 2010 anthropogenic emissions. In AGU Fall Meeting Abstracts 2012 Dec.
- 20 | **Kleffmann, J.: Daytime sources of nitrous acid (HONO) in the atmospheric boundary layer,
21 | *Chemistry and Physical Chemistry*, 8(8), 1137-1144, 2007.**
- 22 | Kumar, P., and Imam, B.: Footprints of air pollution and changing environment on the
23 | sustainability of built infrastructure, *Science of the Total Environment*, 444, 85-101,
24 | 10.1016/j.scitotenv.2012.11.056, 2013.
- 25 | Kurokawa, J., Ohara, T., Morikawa, T., Hanayama, S., Janssens-Maenhout, G., Fukui, T.,
26 | Kawashima, K., and Akimoto, H.: Emissions of air pollutants and greenhouse gases over
27 | Asian regions during 2000–2008: Regional Emission inventory in ASia (REAS) version 2,
28 | *Atmospheric Chemistry and Physics*, 13(21), 11019-11058, 2013.
- 29 | Lam, S. H. M., Saunders, S. M., Guo, H., Ling, Z. H., Jiang, F., Wang, X. M., and Wang, T.
30 | J.: Modelling VOC source impacts on high ozone episode days observed at a mountain

1 summit in Hong Kong under the influence of mountain-valley breezes, *Atmospheric*
2 *Environment*, 81, 166-176, 10.1016/j.atmosenv.2013.08.060, 2013.

3 | Lefohn, A. S., Shadwick, D., and Oltmans, S. J.: Characterizing changes in surface ozone
4 levels in metropolitan and rural areas in the United States for 1980-2008 and 1994-2008,
5 *Atmospheric Environment*, 44, 5199-5210, 2010.

6 | Li, J. F., Lu, K. D., Lv, W., Li, J., Zhong, L. J., Ou, Y. B., Chen, D. H., Huang, X., and
7 Zhang, Y. H.: Fast increasing of surface ozone concentrations in Pearl River Delta
8 characterized by a regional air quality monitoring network during 2006-2011, *Journal of*
9 *Environmental Science -China*, 26, 23-36, 2014.

10 | Li, Z. Y., Xue, L. K., Yang, X., Zha, Q. Z., Tham, Y. J., Yan, C., Louie, P. K. K., Luk, C. W.
11 Y., Wang, T., and Wang, W. X.: Oxidizing capacity of the rural atmosphere in Hong Kong,
12 Southern China, *Science of the Total Environment*, 612, 1114-1122,
13 10.1016/j.scitotenv.2017.08.310, 2018.

14 | Lin, M. Y., Horowitz, L. W., Payton, R., Fiore, A. M., and Tonnesen, G.: US surface ozone
15 trends and extremes from 1980 to 2014: quantifying the roles of rising Asian emissions,
16 domestic controls, wildfires, and climate, *Atmospheric Chemistry and Physics*, 17, 2943-
17 2970, 10.5194/acp-17-2943-2017, 2017.

18 | Ling, Z. H., Guo, H., Lam, S., Saunders, S., and Wang, T.: Atmospheric photochemical
19 reactivity and ozone production at two sites in Hong Kong: Application of a Master Chemical
20 Mechanism–photochemical box model, *Journal of Geophysical Research - Atmospheres*, 119,
21 10567-10582, 2014.

22 | Ling, Z. H., Guo, H., Zheng, J. Y., Louie, P. K. K., Cheng, H. R., Jiang, F., Cheung, K.,
23 Wong, L. C., and Feng, X. Q.: Establishing a conceptual model for photochemical ozone
24 pollution in subtropical Hong Kong, *Atmospheric Environment*, 76, 208-220,
25 10.1016/j.atmosenv.2012.09.051, 2013.

26 | Liu, H., and Chan, J. C. L.: An investigation of air-pollutant patterns under sea–land breezes
27 during a severe air-pollution episode in Hong Kong, *Atmospheric Environment* 36, 591–601,
28 2002.

29 | Liu, K.-Y., Wang, Z., and Hsiao, L.-F.: A modeling of the sea breeze and its impacts on
30 ozone distribution in northern Taiwan, *Environmental Modelling & Software*, 17, 21-27,
31 2002.

- 1 | Lo, J. C. F., Lau, A. K. H., Fung, J. C. H., and Chen, F.: Investigation of enhanced cross-city
2 | transport and trapping of air pollutants by coastal and urban land-sea breeze circulations,
3 | *Journal of Geophysical Research-Atmospheres*, 111, 2006.
- 4 | Lu, K. D., Zhang, Y. H., Su, H., Shao, M., Zeng, L. M., Zhong, L. J., Xiang, Y. R., Chang, C.
5 | C., Chou, C. K. C., and Wahner, A.: Regional ozone pollution and key controlling factors of
6 | photochemical ozone production in Pearl River Delta during summer time, *Science China*
7 | *Chemistry*, 53, 651-663, 10.1007/s11426-010-0055-6, 2010.
- 8 | Lu, X., Chow, K.-C., Yao, T., Lau, A. K. H., and Fung, J. C. H.: Effects of urbanization on
9 | the land sea breeze circulation over the Pearl River Delta region in winter, *International*
10 | *Journal of Climatology*, n/a-n/a, 10.1002/joc.1947, 2009a.
- 11 | Lu, X., Chow, K. C., Yao, T., Fung, J. C. H., and Lau, A. K. H.: Seasonal variation of the
12 | land-sea breeze circulation in the Pearl River Delta region, *Journal of Geophysical Research-*
13 | *Atmospheres*, 114, 2009b.
- 14 | Monks, P. S., Archibald, A. T., Colette, A., Cooper, O., Coyle, M., Derwent, R., Fowler, D.,
15 | Granier, C., Law, K. S., Mills, G. E., Stevenson, D. S., Tarasova, O., Thouret, V., Von
16 | Schneidemesser, E., Sommariva, R., Wild, O., and Williams, M. L.: Tropospheric ozone and
17 | its precursors from the urban to the global scale from air quality to short-lived climate forcer,
18 | *Atmospheric Chemistry and Physics*, 15, 8889-8973, 10.5194/acp-15-8889-2015, 2015.
- 19 | NARSTO: An Assessment of Tropospheric Ozone Pollution-A North American Perspective,
20 | NARSTO Management Office (Envair), Pasco, Washington, 2000.
- 21 | NRC: Rethinking the Ozone Problem in Urban and Regional Air Pollution, National
22 | Research Council, 1991.
- 23 | Parrish, D. D., Trainer, M., Holloway, J. S., Yee, J. E., Warshawsky, M. S., Fehsenfeld, F. C.,
24 | Forbes, G. L., and Moody, J. L.: Relationships between ozone and carbon monoxide at
25 | surface sites in the North Atlantic region, *Journal of Geophysical Research-Atmospheres*, 103,
26 | 13357-13376, 1998.
- 27 | Parrish, D. D., Law, K. S., Staehelin, J., Derwent, R., Cooper, O. R., Tanimoto, H., Volz-
28 | Thomas, A., Gilge, S., Scheel, H. E., Steinbacher, M., and Chan, E.: Long-term changes in
29 | lower tropospheric baseline ozone concentrations at northern mid-latitudes, *Atmospheric*
30 | *Chemistry and Physics*, 12, 11485-11504, 2012.

1 | Ran, L., Zhao, C. S., Xu, W. Y., Lu, X. Q., Han, M., Lin, W. L., Yan, P., Xu, X. B., Deng, Z.
2 | Z., Ma, N., Liu, P. F., Yu, J., Liang, W. D., and Chen, L. L.: VOC reactivity and its effect on
3 | ozone production during the HaChi summer campaign, *Atmospheric Chemistry and Physics*,
4 | 11, 4657-4667, 10.5194/acp-11-4657-2011, 2011.

5 | Saunders, S. M., Jenkin, M. E., Derwent, R. G., and Pilling, M. J.: Protocol for the
6 | development of the Master Chemical Mechanism, MCM v3 (Part A): tropospheric
7 | degradation of non-aromatic volatile organic compounds, *Atmospheric Chemistry and*
8 | *Physics*, 3, 161-180, 2003.

9 | Seinfeld, J. H., and Pandis, S. N.: *Atmospheric chemistry and physics: from air pollution to*
10 | *climate change*, John Wiley & Sons, 2016.

11 | Shindell, D., Kuylensstierna, J. C. I., Vignati, E., van Dingenen, R., Amann, M., Klimont, Z.,
12 | Anenberg, S. C., Muller, N., Janssens-Maenhout, G., Raes, F., Schwartz, J., Faluvegi, G.,
13 | Pozzoli, L., Kupiainen, K., Hoglund-Isaksson, L., Emberson, L., Streets, D., Ramanathan, V.,
14 | Hicks, K., Oanh, N. T. K., Milly, G., Williams, M., Demkine, V., and Fowler, D.:
15 | Simultaneously Mitigating Near-Term Climate Change and Improving Human Health and
16 | Food Security, *Science*, 335, 183-189, 10.1126/science.1210026, 2012.

17 | Simpson, I. J., Blake, N. J., Barletta, B., Diskin, G. S., Fuelberg, H. E., Gorham, K., Huey, L.
18 | G., Meinardi, S., Rowland, F. S., Vay, S. A., Weinheimer, A. J., Yang, M., and Blake, D. R.:
19 | Characterization of trace gases measured over Alberta oil sands mining operations: 76
20 | speciated C-2-C-10 volatile organic compounds (VOCs), CO₂, CH₄, CO, NO, NO₂, NO_y, O₃
21 | and SO₂, *Atmospheric Chemistry and Physics*, 10, 11931-11954, 2010.

22 | Skamarock, W. C., Klemp, J. B., Dudhia, J., Gill, D. O., Barker, D. M., Duda, M. G, Huang,
23 | X.-Y., Wang, W., and Powers, J. G.: A Description of the Advanced Research WRF Version
24 | 3. NCAR Tech. Note NCAR/TN-475+STR, 113 pp. doi:10.5065/D68S4MVH, 2008.

25 | Stein, A.F., Draxler, R.R, Rolph, G.D., Stunder, B.J.B., Cohen, M.D., and Ngan, F.: NOAA's
26 | HYSPLIT atmospheric transport and dispersion modeling system, *Bulletin of American*
27 | *Meteorological Society*, 96, 2059-2077, 2015.

28 | Sun, L., Xue, L. K., Wang, T., Gao, J., Ding, A. J., Cooper, O. R., Lin, M. Y., Xu, P. J.,
29 | Wang, Z., Wang, X. F., Wen, L., Zhu, Y. H., Chen, T. S., Yang, L. X., Wang, Y., Chen, J. M.,
30 | and Wang, W. X.: Significant increase of summertime ozone at Mount Tai in Central Eastern

- 1 [China, Atmospheric Chemistry and Physics, 16, 10637-10650, 10.5194/acp-16-10637-2016,](#)
2 [2016.](#)
- 3 | Velchev, K., Cavalli, F., Hjorth, J., Marmer, E., Vignati, E., Dentener, F., and Raes, F.:
4 | Ozone over the Western Mediterranean Sea – results from two years of shipborne
5 | measurements, *Atmospheric Chemistry and Physics*, 11, 675-688, 10.5194/acp-11-675-2011,
6 | 2011.
- 7 | Wang, N., Guo, H., Jiang, F., Ling, Z. H., and Wang, T.: Simulation of ozone formation at
8 | different elevations in mountainous area of Hong Kong using WRF-CMAQ model, *Science*
9 | *of the Total Environment*, 505, 939-951, 2015.
- 10 | Wang, T., LAM, K. S., and LEE, A. S. Y.: Meteorological and Chemical Characteristics of
11 | the Photochemical Ozone Episodes Observed at Cape D’Aguilar in Hong Kong, *Journal of*
12 | *Applied Meteorology*, 30, 1167-1178, 1998.
- 13 | Wang, T., Guo, H., Blake, D. R., Kwok, Y. H., Simpson, I. J., and Li, Y. S.: Measurements of
14 | Trace Gases in the Inflow of South China Sea Background Air and Outflow of Regional
15 | Pollution at Tai O, Southern China, *Journal of Atmospheric Chemistry*, 52, 295-317,
16 | 10.1007/s10874-005-2219-x, 2005.
- 17 | Wang, T., Wei, X. L., Ding, A. J., Poon, C. N., Lam, K. S., Li, Y. S., Chan, L. Y., and Anson,
18 | M.: Increasing surface ozone concentrations in the background atmosphere of Southern China,
19 | 1994-2007, *Atmospheric Chemistry and Physics*, 9, 6217-6227, 2009.
- 20 | Wang, Y., Guo, H., Zou, S., Lyu, X., Wang, H., Ling, Z., and Cheng, H.: Ground level O₃
21 | photochemistry over South China Sea: Application of a near-explicit chemical mechanism
22 | box model, *Environmental Pollution*, under revision, 2017b.
- 23 | Wang, Y., Wang, H., Guo, H., Lyu, X., Cheng, H., Ling, Z., Louie, P. K. K., Simpson, I. J.,
24 | Meinardi, S., and Blake, D. R.: Long term O₃-precursor relationships in Hong Kong: Field
25 | observation and model simulation, *Atmospheric Chemistry and Physics*, 17(18), 10919-
26 | 10935, 2017a.
- 27 | Wei, X., Lam, K.-S., Cao, C., Li, H., and He, J.: Dynamics of the Typhoon Haitang Related
28 | High Ozone Episode over Hong Kong, *Advances in Meteorology*, 2016, 1-12,
29 | 10.1155/2016/6089154, 2016.

- 1 | WHO: Health aspects of air pollution with particulate matter, ozone and nitrogen dioxide:
2 | report on a WHO working group, Bonn, Germany 13-15 January 2003, World Health
3 | Organization, 2003.
- 4 | Willmott, C. J.: Some comments on the evaluation of model performance, *Bulletin of the*
5 | *American Meteorological Society*, 63(11), 1309-1313, 1982.
- 6 | Xu, X., Lin, W., Wang, T., Yan, P., Tang, J., Meng, Z., and Wang, Y.: Long-term trend of
7 | surface ozone at a regional background station in eastern China 1991-2006: enhanced
8 | variability, *Atmospheric Chemistry and Physics*, 8, 2595-2607, 2008.
- 9 | Xu, Z., Wang, T., Wu, J., Xue, L., Chan, J., Zha, Q., Zhou, S., Louie, P.K.K., and Luk, C. W.:
10 | Nitrous acid (HONO) in a polluted subtropical atmosphere: Seasonal variability, direct
11 | vehicle emissions and heterogeneous production at ground surface, *Atmospheric environment*,
12 | 106, 100-109, 2015.
- 13 | Xue, L. K., Wang, T., Louie, P. K. K., Luk, C. W. Y., Blake, D. R., and Xu, Z.: Increasing
14 | External Effects Negate Local Efforts to Control Ozone Air Pollution: A Case Study of Hong
15 | Kong and Implications for Other Chinese Cities, *Environmental Science and Technology*, 48,
16 | 10769-10775, 10.1021/es503278g, 2014.
- 17 | Xue, L., Gu, R., Wang, T., Wang, X., Saunders, S., Blake, D., Louie, P.K.K., Luk, C.W.Y.,
18 | Simpson, I., Xu, Z., Wang, Z., Gao Y., Lee, S., Mellouki, A., and Wang, W.: Oxidative
19 | capacity and radical chemistry in the polluted atmosphere of Hong Kong and Pearl River
20 | Delta region: analysis of a severe photochemical smog episode, *Atmospheric Chemistry and*
21 | *Physics*, 16, 9891-9903, 2016.
- 22 | Yang, J. X., Lau, A. K. H., Fung, J. C. H., Zhou, W., and Wenig, M.: An air pollution episode
23 | and its formation mechanism during the tropical cyclone Nuri's landfall in a coastal city of
24 | south China, *Atmospheric Environment*, 54, 746-753, 10.1016/j.atmosenv.2011.12.023, 2012.
- 25 | Yin, L. H.: Analysis of Meteorological Criteria Leading to Tropical Cyclone Related Ozone
26 | Episodes in Hong Kong, PhD, HKUST, 2004.
- 27 | Zha, Q.: Measurement of nitrous acid (HONO) and the implications to photochemical
28 | pollution (MPhil dissertation, The Hong Kong Polytechnic University), 2015.
- 29 | Zhang, M., and Zhang, L.: Study of the sea-land breeze system in Hong Kong, *Hong Kong*
30 | *Meteorological Society Bulletin*, 22-42, 1997.

1 | Zhang, Q., Yuan, B., Shao, M., Wang, X., Lu, S., Lu, K., Wang, M., Chen, L., Chang, C. C.,
2 | and Liu, S. C.: Variations of ground-level O₃ and its precursors in Beijing in summertime
3 | between 2005 and 2011, *Atmospheric Chemistry and Physics*, 14, 6089-6101, 10.5194/acp-
4 | 14-6089-2014, 2014.

5 | Zheng, J. Y., Zhong, L. J., Wang, T., Louie, P. K. K., and Li, Z. C.: Ground-level ozone in
6 | the Pearl River Delta region: Analysis of data from a recently established regional air quality
7 | monitoring network, *Atmospheric Environment*, 44, 814-823, 2010.

8 |
9 |